Magnetic field and voltage noise in type-II superconductors

B. Plaçais, P. Mathieu, and Y. Simon
Laboratoire de Physique de la Matière Condensée de l'Ecole Normale Supérieure, F-75231 Paris Cédex 05, France
(Received 10 January 1994)

The puzzling problem of flux-flow noise is investigated both theoretically and experimentally. Combined measurements of the voltage noise and magnetic flux noise in various search coils have been performed, using the classical geometry of soft long strips in a perpendicular field. Our samples are immersed in superfluid helium ($T \sim 1.8$ K), allowing one to widely explore the flux-flow regime. Auto and cross spectra, in the $1-10^4$ Hz range, provide decisive information about the possible sources of noise. In particular, experimental results cannot be reconciled with a two-dimensional (2D) picture of the vortex motion, especially with the classical shot-noise model. A recently presented 3D mechanism of noise [Phys. Rev. Lett. **70**, 1521 (1993)] is discussed at greater length in this paper. According to a continuum theory of transport in type-II superconductors by two of us (P.M. and Y.S.), the transport current **J** is separated into a nondissipative surface current $\mathbf{J}_1$ and a bulk dissipative current $\mathbf{J}_2$. The former is associated with the instantaneous distorted configuration of the vortex array, whereas the latter is connected with its motion. A model is developed, that describes surface currents as a 2D homogeneous turbulent flow. This is characterized locally by its normalized spectrum $\Sigma(f)$, the intensity of the turbulence—denoted as $u^*(\sim 10^2$ A/m) in the text, and directly related to the critical current density—and a correlation length $c \sim 1-3$ μm. Auto or cross spectra of both voltage and magnetic field noises can be entirely predicted as a function of $\Sigma(f)$, u^*, and c, in full agreement with experiment.

I. INTRODUCTION

Van Ooijen and Van Gurp,[1,2] put noise measurements forward as a well-suited tool to investigate the vortex dynamics in the flux-flow regime. Flux-flow noise (FFN) indeed should reveal the more or less irregular motion of the vortices, and provide information about the spatial distribution of the moving vortex array. In their original model, the so-called shot-noise model, they advanced the idea that the noise voltage δV across the sample was due to flux bundles being nucleated randomly at one edge of the sample and moved rigidly across the sample at constant velocity $\mathbf{v}_L$. This model implies strong vortex-density fluctuations δn_L. Taking a different view, Heiden *et al.*[3] considered that the FFN, in particular in pure metals (V,Nb), may well result from velocity fluctuations $\delta \mathbf{v}_L$ in the vicinity of pinning sites, in an otherwise quasi-perfect moving lattice ($\delta n_L \simeq 0$).

Following the pioneering work of Van Ooijen and Van Gurp, a number of theoretical and experimental FFN studies have been published during the 1970's.[3-13] The reader is referred to the critical review by Clem.[14] Most experiments consisted in measuring autopower spectra of δV (with a single contact pair): typically $10^{-8}-10^{-11}$ V/Hz$^{1/2}$ in the 0–10 kHz bandwidth. A few authors also have investigated the magnetic-field noise around the sample,[7-9] by measuring the noisy magnetic flux $\delta\Phi(t)$ through variously shaped pickup coils. Still more rarely, cross-correlation measurements between two noisy variables have been reported in the FFN literature: Using two movable contact pairs, Heiden *et al.*[3] measured cross-correlation functions of two voltages; Choe *et al.*[7] are concerned with the correlations between δV and $\delta\Phi$ through two rectangular loops adjoining the sample. It should be noted that noise experiments have been performed on a rather restricted class of conventional type-II superconductors, viz. lead alloys (PbIn)[8-11] or pure metals (Nb,V).[1-7] Samples are made from soft materials, and have low-to-moderate critical currents. They are shaped as foils or thin strips perpendicular to the applied magnetic field, and have typically 1–5 cm length, 1–5 mm width, and 20–200 μm thickness.

Unfortunately all these works have not led to a coherent picture of FFN, and, although powerful and promising, the cross-correlation technique has not clarified the problem. As noticed already by Campbell in 1972:[15] "While noise measurements are certainly measuring an important parameter, its relationship to the way in which flux moves remains rather obscure." Experiments seemed to be contradictory, and lent themselves to varied interpretations, each of them involving a number of adjustable parameters. Most of them are attempts to improve the initial shot-noise model.[6-11] The principal parameter in a shot-noise model is the flux-bundle size φ_b; some critical-current models, still brought forward in topical discussions about high-T_c materials (thermally activated flux creep), rely on this concept of bundle, introduced by Anderson.[16] One might have expected that noise measurements would provide a clear evidence of the existence of bundles. Instead, voltage noise measurements have brought the matter to a great confusion: Somewhat artificially, φ_b is found to be a rapidly decreasing function of current by several orders of magnitude, from about 10^4 φ_0 down to the flux quantum φ_0,[11] while the amplitude of noise itself was rather stationary. In pure metals, φ_b even happens to fall below the flux quantum.[4] Just this fact prompted Heiden *et al.* to ascribe

0163-1829/94/49(22)/15813(17)/$06.00

FFN to fluctuations of the vortex velocity, but with no great success. As a matter of fact, the mechanism involved in alloys and pure metals is quite similar, and the relative smallness of the voltage noise in pure niobium (Sec. VI B) will follow immediately from our interpretation of δV in Sec. III C.

The attempt at a comprehensive analysis of FFN in a general theoretical frame is due to Clem.[14] In Clem's description, flux flow is regarded as a two-dimensional (2D) vortex motion. Introducing a vortex-current density $\mathbf{J}_L = n_L \mathbf{v}_L$ (labeled **J** in Ref. 14), all the useful information about the dynamical behavior of the vortex array is contained in the 2D vortex-current correlation tensor $K_{\alpha\beta}$. As a concluding remark of his substantial review of experimental results, Clem states that "the remaining task for developing a suitable theory for $K_{\alpha\beta}$ is likely to be challenging." Then he adds that "such a theory should be intimately related to an appropriate theory for the critical current density." While a 2D model turns out to be inadequate, as argued at great length below, Clem's latter remark was prophetic of the noise theory propounded in this paper. We indeed believe that a 3D analysis of the current distribution, where the critical current will appear as a well-defined and fluctuating part of the transport current, is just the key to the puzzle of FFN.

We have reexamined the problem of noise, both theoretically and experimentally.[17] We have performed a series of experiments *in superfluid helium* ($T \simeq 1.8$ K), in order to avoid spurious sources of noise, such as the flicker noise, due to excessive dissipation. In this way, we can widely explore the flux-flow regime. At the onset of the *I-V* curve, flux flow is essentially inhomogeneous along the sample, and noise measurements yield unreliable results. By relying on a phenomenological theory of vortex motion, we shall refer to below as the Mathieu and Simon (MS) theory[18,19] (see Sec. III), we were able to work out a consistent theory of FFN (Sec. IV), the principle of which has been reported in a recent letter.[20] In this paper we report, as a proof, field- and voltage-noise measurements in various geometries, by taking systematic advantage of the powerful technique of cross correlations. Their purpose is to *identify* and *localize* the sources of noise unambiguously, and to elucidate the mechanism giving rise to voltage noise. In tackling the FFN literature, there may be a general feeling that each new experiment called for its own *ad hoc* interpretation. We emphasize in this respect, that we can endorse past experiments as well, as they all are accounted for by our model: as an example two results obtained, respectively, by Jarvis and Park[8] and Choe and Van der Ziel[7] are discussed in Sec. VI D.

II. MACROSCOPIC ANALYSIS OF THE FLUX-FLOW NOISE

We cannot reasonably treat 3D motions of the vortex array, without regarding it as a continuum, and using macroscopic or cross-grained mean values $\mathbf{J} = \langle \mathbf{j} \rangle$, $\mathbf{E} = \langle \mathbf{e} \rangle$, $\mathbf{B} = \langle \mathbf{b} \rangle$ of currents and fields. Macroscopic (or microscopic) here means on a large (or small) scale compared with the vortex spacing a. Note that in experiments we only have access to these macroscopic fields.

Consider a voltage measuring circuit consisting of two leads *ma* and *mb* connecting contacts *a* and *b* on a superconducting strip as shown in Fig. 1. The sample is immersed in a constant normal magnetic field $\mathbf{B}_0$ and is driven in the flux-flow regime by a constant applied current I. Closing the loop by any convenient path (*asb*) through the sample, the measured voltage V can be written as the sum of two terms:[14]

$$V = \int_{asb} \mathbf{E} \cdot \mathbf{dl} - \frac{\partial \phi_{ms}}{\partial t} , \tag{1}$$

where ϕ_{ms} is the flux of **B** through the loop (*ambsa*). The result (1) is independent of which path (*asb*) is taken. Clem starts from Eq. (1), expressed in terms of microscopic fields,[14] to calculate the contribution to V of an individual moving vortex. But any equation in electromagnetics of continuous media indeed may be written in terms of either microscopic or macroscopic fields. In using macroscopic variables we shall take advantage of the relationship between **E** and $\mathbf{v}_L$ (under quasistationary conditions):[18]

$$\mathbf{E} = -\mathbf{v}_L \times \boldsymbol{\omega} , \tag{2}$$

where $\boldsymbol{\omega} = n_L \varphi_0 \boldsymbol{\nu}$ is a vector which describes the local density and direction $\boldsymbol{\nu}$ of vortex lines.[18] As pointed out by MS,[18] the equality $\boldsymbol{\omega} = \mathbf{B}$ fails in regions where supercurrents are not curlfree, in particular over a small depth $d \sim a$ from the surface [see Eq. (7)]. This distinction will become important when analyzing surface-current fluctuations. Now, for merely calculating V, the path (*asb*) can be chosen so as to penetrate into the sample and run beyond the perturbed layer d. For such a path (*asb*), Eq. (2) may be used in its well-known common form $\mathbf{E} = -\mathbf{v}_L \times \mathbf{B}$.

Thus, on substituting $\mathbf{E} = -\mathbf{v}_L \times \mathbf{B}$ in Eq. (1), the voltage noise δV can be analyzed as a sum of three terms, as

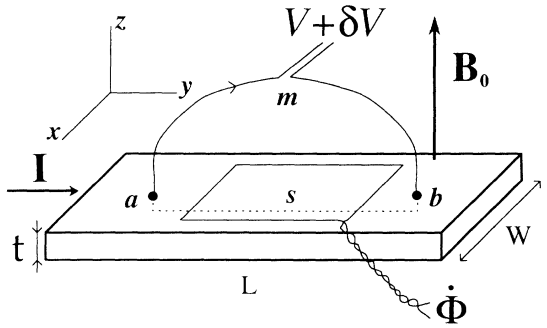

FIG. 1. The classical geometry of a slab in perpendicular field, such as used in noise measurements. Actually $t \ll W \ll L$. In a constant external field B_0, and at constant applied current I, both the voltage noise δV across the sample and the induced noise $\dot{\Phi}$ through variously shaped pickup coils, reveal the irregular motion of vortices throughout the slab. For the sake of the discussion a coordinate system has been chosen by taking the origin at the center of the slab (not shown), and directions of axis as indicated in the figure.

function of the field noise $\delta\mathbf{B}$ and the velocity noise $\delta\mathbf{v}_L$:

$$\delta V=\int_{ab}(\mathbf{B}\times\delta\mathbf{v}_L)\cdot\mathbf{d}l+\int_{ab}(\delta\mathbf{B}\times\mathbf{v}_L)\cdot\mathbf{d}l -\frac{\partial}{\partial t}\int\int_{ms}\delta\mathbf{B}\cdot\mathbf{d}\sigma \ . \tag{3}$$

In differentiating $\mathbf{B}\times\mathbf{v}_L$, we have implicitly assumed, in agreement with experiment, that $\delta\mathbf{B}$ (see Sec. VI) and $\delta\mathbf{v}_L$ are relatively small fluctuations. Nevertheless, Eq. (3) still holds in shot-noise models, which involve large $\delta\mathbf{B}\sim\mathbf{B}$ at constant $\mathbf{v}_L$.

It is worth determining which terms are prevailing in δV. In particular the contribution of the field noise in the last two terms of Eq. (3) can be estimated from independent measurements of the magnetic flux $\delta\Phi$ induced in pickup coils. For example, Jarvis and Park attempted to measure in this way the third term $\dot{\phi}_{ms}$.[8,14] More quantitative information will be gained by simultaneous measurements of auto and cross power spectra of voltage and field noises, denoted below as S_{VV}, $S_{\phi\phi}$, and $S_{V\phi}(f)$. In our experiments, cross correlation between voltage and field noises have proved to be useful in deciding between competitive models. As far as we know, Choe and Van der Ziel alone reported earlier measurements of $S_{V\phi}$.[7] These authors failed to conclude, however, since they relied on the shot-noise model. Their results will be discussed in Sec. VI D.

It is obvious that any field noise $\delta\mathbf{B}$, in the usual low-frequency range, has to be associated, through Ampere's theorem or Biot-Savart law, with a noisy distribution of currents ($\mu_0\delta\mathbf{J}=\text{curl}\delta\mathbf{B}$). As discussed in Sec. III, it will be more advisable, in a 3D continuum description of the FFN, to regard the current density fluctuations $\delta\mathbf{J}$ as the primary sources of noise. Therefore, by measuring the magnetic flux noise $\delta\Phi$ in a variety of coils around the sample (auto and cross correlations), rather direct information is obtained about these sources. In spite of the smallness of induced signals, field-noise measurements will be an essential tool to disentangle noise data. Though still significant, the noise voltage will appear instead as an indirect and more intricate consequence of the FFN.

It is instructive to show that Clem's results can be derived from the above formalism as a particular case of application. Clem confines himself to strictly *2D vortex motions* and relies on a principle of superposition of currents and fields due to individual vortices. Taking xyz axes as shown in Fig. 1, $\nu(0,0,1)=\text{const}$, while $n_L(x,y)$ and $\mathbf{v}_L(v_{Lx},v_{Ly},0)$ fluctuate according to any particular model. Clem has shown that V can be merely expressed as a function of the vortex-current density $\mathbf{J}_L=n_L\mathbf{v}_L$ in the form[14]

$$V=\int\int\mathbf{g}\cdot\mathbf{J}_L dx\,dy \ , \quad \text{(2D motions)} \ , \tag{4}$$

where $\mathbf{g}(x,y)$ is a resolving function depending on the geometry of the measuring circuit (amb).

In Appendix A, Eq. (4) is derived from Eqs. (1) and (2). It is shown that the resolving function $\mathbf{g}$ can be written as $-\nabla f$, where $f(x,y)$ is the magnetic flux ($-\varphi_0\le f\le\varphi_0$) through the measuring circuit due to one vortex at a point (x,y).

Shot-noise models are concerned with 2D motions at constant $\mathbf{v}_L(v_L,0,0)$. In this case, Eq. (4) yields

$$V(t)=v_L\int\int g_x n_L(\mathbf{r},t)dx\,dy \ . \tag{5}$$

For a long strip ($W\ll L$), to which voltage leads are attached to the ends ($ab\sim L$) while passing far enough from the surface ($z\gtrsim W$), $g_x(x)\sim\varphi_0/W$ so that[14]

$$V(t)\sim\frac{v_L}{W}\phi_s(t) \ , \quad \text{(shot-noise)} \ , \tag{6}$$

where $\phi_s(t)$ is the noisy magnetic flux through the sample. This simple result, which is independent of any fitting parameters, implies a strong correlation between the voltage noise δV and the field noise $\delta\phi_s$ through a rectangular loop $L\times W$ around the sample. From the observed order of magnitude of δV (10^{-17} V^2/Hz), and taking typical values $v_L/W\sim10^2$ Hz, Eq. (6) predicts large field noise $\delta\phi_s$ ($10^8\varphi_0^2$/Hz). This close relationship between δV and $\delta\phi_s$, which characterizes shot-noise mechanisms, has not been pointed out in the noise literature. We return to this point in discussing experimental results (Sec. VI B).

III. VORTEX AND CURRENT DISTRIBUTION IN THE FLUX-FLOW REGIME AND THE NOISE MECHANISM

A. The MS theory

A mechanism for the FFN follows at once from the MS model for critical currents in soft materials,[19] which itself proceeds from their phenomenological theory of vortex motion.[18] In the MS theory, the mixed state is regarded as a continuum. The local mean density of free energy F is expressed as a function of a reduced set of thermodynamic variables, in particular the macroscopic fields $\mathbf{E}$, $\mathbf{B}$, the mean supercurrent $\mathbf{J}_s$ (or the superfluid velocity $\mathbf{V}_s$), and ω. One essential point in the MS theory is to realize from the outset that ω and $\mathbf{B}$ must be considered as local independent variables: for a given value of ω at some point M, $\mathbf{B}(M)$ still may be varied by any change in the distribution of currents elsewhere. The macroscopic London equation states that[18,19]

$$\omega=\mathbf{B}-m/e\ \text{curl}\mathbf{V}_s \ , \tag{7}$$

where m and $-e$ are the electronic mass and charge. From Eq. (7) it is seen that $\omega=\mathbf{B}$ in regions where supercurrents are curlfree (in particular where $\mathbf{J}_s\equiv0$). A vortex potential is defined as $\varepsilon=\partial F/\partial\omega$. The equation of state, $\varepsilon(\omega,T)$, is directly related to the usual reversible magnetization curve.[19]

Firstly, the equations for thermodynamic equilibrium are obtained by minimizing the appropriate magnetic free enthalpy. In particular,[19]

$$\mathbf{J}=\mathbf{J}_s=-\text{curl}\ \varepsilon \ , \tag{8}$$

$$\varepsilon\times\mathbf{N}=0 \ , \tag{9}$$

where $\mathbf{N}$ is the outward normal unit vector. Equation (8),

or $\mathbf{J}_s + \mathrm{curl}\varepsilon = 0$, states, in a macroscopic way, that the supercurrent at the vortex cores is zero, including the contribution induced by vortices themselves if they are curved. Since in rather general conditions $\varepsilon \simeq \varepsilon \boldsymbol{\nu}$ is along vortex lines, Eq. (9) means that vortex lines (defined as the lines $\psi = 0$) must terminate perpendicular to the sample surface. According to Eq. (8), a systematic bending of vortex lines can exist at equilibrium, say in the xz planes, provided that a supercurrent flows in the y direction.

On combining Eqs. (7), (8), and (9), and Maxwell equations, it is easily shown that such a distortion of the vortex array takes place, and associated $\mathbf{J}_s$ flow, only over a small depth $d \sim a$ from the surface, while $\mathbf{J}_s \simeq 0$ and $\boldsymbol{\omega} \simeq \mathbf{B}$ in the bulk.[19] In ideal samples, these supercurrents, associated with the local bending of the vortices, are nothing but Meissner-like diamagnetic currents.[19]

Now, consider the case of a rough slab in a perpendicular field (Figs. 1 and 2): there are no diamagnetic currents. But in the presence of surface roughness on a scale comparable to or smaller than the vortex spacing a, there are many ways for the vortices to end normal to the actual surface, allowing for a large number of metastable or nondissipative solutions. Associated supercurrents in this case may well superpose, to give rise to a nondissipative transport current. In principle, a continuum description excludes inhomogeneities at the scale of a. However, to make allowance for unavoidable surface defects in the frame of a continuum model, MS suggest that Eq. (9) should be replaced by an inequality in the form

$$|\varepsilon \times \mathbf{N}| \leq \varepsilon \sin\theta_c \ , \tag{10}$$

where $\mathbf{N}$ now is the normal to the mean smoothed surface (Fig. 2). This new boundary condition enables a net transport current i (A/m) to flow near the surface up to a critical value i_c. Integrating Eq. (8) over the depth d, we find

$$\mathbf{i} = \varepsilon \times \mathbf{N} \ . \tag{11}$$

In the critical state, $i_y = -\varepsilon \nu_x = \varepsilon \sin\theta_c = i_c$ so that

$$I_c \approx 2W\varepsilon \sin\theta_c = 2Wi_c \ . \tag{12}$$

Taking for ε, as a first good approximation, the bulk value $\varepsilon(\omega, T)$, and $\sin\theta_c \lesssim 1$ ($\theta_c \sim 10°$) we were able to account for the magnitude of critical currents *in soft samples* as well as their temperature and field dependence.[21]

When the current density $\mathbf{J}$ departs from $-\mathrm{curl}\varepsilon$, the vortex array moves. So it is convenient to separate $\mathbf{J}$ into two parts as

$$\mathbf{J} = \mathbf{J}_1 + \mathbf{J}_2 \ , \tag{13}$$

where $\mathbf{J}_1 = -\mathrm{curl}\varepsilon$ is the nondissipative part of the current.[19] $\mathbf{J}_1$ is defined, at any point and time, as the supercurrent that would come into equilibrium with the vortex array in its instantaneous configuration (Fig. 2).

Using a standard rigorous method, MS derived a complete set of transport equations. In quasistationary conditions, covering ac transport currents in the acoustic range of frequencies and the whole investigated spectrum of FFN, the MS transport equations take a simplified form: In addition to Eq. (2), there is a simple relationship between the line velocity $\mathbf{v}_L$ and the dissipative current

$$\frac{\rho_f}{\omega}\mathbf{J}_{2\perp} = -\mathbf{v}_L \times \boldsymbol{\nu} \ , \tag{14}$$

where $\rho_f(\omega)$ is the flux-flow resistivity. From Eqs. (2) and (14) we have

$$\mathbf{E} = -\mathbf{v}_L \times \boldsymbol{\omega} = \rho_f \mathbf{J}_{2\perp} \ . \tag{15}$$

Whereas currents $\mathbf{J}_1$ may be regarded as idealized surface currents $\mathbf{i}_1$ (i_1 A/m) on the scale of the sample, currents $\mathbf{J}_2$ are bulk distributed. Note that $\mathbf{J}_1$, as also the component of $\mathbf{J}_2$ along $\boldsymbol{\nu}$, do not contribute to the dissipative function.

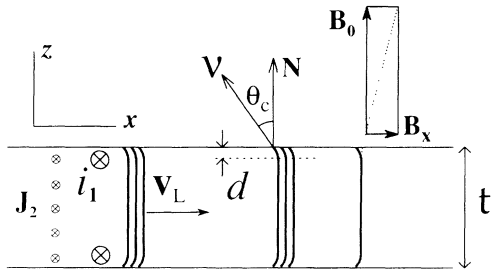

FIG. 2. A time-average picture of the vortex flow, and schematic of the current distribution according to the MS model (Sec. III A). Owing to surface irregularities on the scale of the vortex spacing (not shown), many configurations of the vortex array near the surface should exist. Vortex lines can be bent over a thin layer d ($\xi \lesssim d \lesssim \lambda$) so as to make a maximum angle θ_c with the normal $\mathbf{N}$ to the mean smoothed surface [Eq. (10)]. Maximum bending of vortices, in the direction indicated in the figure, makes the associated nondissipative currents $\mathbf{J}_1$ [Eq. (8)] flow systematically in the y direction. Whereas currents $\mathbf{J}_1$ may be regarded as surface currents ($\mathbf{i}_1$ A/m), dissipative currents $\mathbf{J}_2$ are uniformly distributed in the bulk. In the perturbed layer, vortex lines are not the magnetic-field lines, in accordance with Eq. (7). Fluctuations of the vortex curvature near the surface and correlative fluctuations of the current partition $\mathbf{J}_1 + \mathbf{J}_2$ are the presumed sources of the flux-flow noise.

B. A model for the flux-flow noise

A picture of the noisy dc flux-flow results from the MS interpretation of pinning in soft samples.[20] The observed shape of the V-I curve at large currents $V = R_f(I - I_c)$, suggests that the surface retains its ability to carry a constant nondissipative current, at least on the average. By assuming that the vortex array moves uniformly, while maintaining its critical-state configuration such as sketched in Fig. 2, MS could explain most of the dc properties; in particular an interpretation of the part VI_c of the dc Joule effect was proposed.[18,19]

Of course, the rigid uniform motion of the vortex array is unrealistic, especially near the surface. It only represents a time-average picture of the vortex flow. While dealing with noise, however, we cannot ignore the irregularities of the vortex flow. The motion of vortex lines passing the surface defects must be very irregular, giving rise to *large local fluctuations of the vortex bending* and associated $\mathbf{J}_1$'s or $\mathbf{i}_1$'s. Thus we expect local $\mathbf{i}_1$ as large

as the mean critical density i_c itself. We regard these fluctuations $\delta \mathbf{i}_1$ of the nondissipative surface current as the primary sources of FFN.

Let $I_1(y,t)$ be the flux of $\mathbf{J}_1$ through any cross section y of the slab. In the flux-flow regime, I_1 appears as a fluctuating part of the total applied current I. We emphasize that, in spite of large local fluctuations of the surface current ($\delta i_1/i_1 \sim 1$), the resulting relative fluctuations $\delta I_1/I_1$ should be considerably reduced by a well-known statistical effect. At constant I, the bulk dissipative current $I_2 = I - I_1$ fluctuates accordingly ($\delta I_2 = -\delta I_1$). Hence we expect fluctuations $\delta \mathbf{J}_2$, which in turn entail fluctuations of the electric field $\delta \mathbf{E}$ (and/or $\delta \mathbf{v}_L$), and therefore voltage noise. In this picture the irregularities of the vortex motion *in the bulk* arise as an indirect consequence of strong perturbations of the vortex array close to the surface.

As stated in Sec. II, the field noise $\delta \mathbf{B}$ indeed results from a noisy distribution of the transport current ($\delta \mathbf{J}_1$ and $\delta \mathbf{J}_2$). Either the mean in-plane components of the field, B_x and B_y ($B_x, B_y \lesssim \mu_0 I/2W \sim 10$ G), or the noisy field components ($\delta B_x, \delta B_y, \delta B_z \lesssim \mu_0 i_c \sim 10$ G), remain relatively small as compared with the field noise predicted by a shot-noise model ($\delta B_z \sim B_z$). In the worked field range 500 G $\lesssim B \lesssim$ 5000 G, this implies that vortex lines *in the bulk*, where $\boldsymbol{\omega} = \mathbf{B}$ ($\delta\boldsymbol{\omega} = \delta\mathbf{B}$), hardly deviate from the main field direction z ($\nu_x, \nu_y \lesssim 10^{-2}$). We stress that strong $\delta\boldsymbol{\omega}$ (or $\delta\boldsymbol{\nu}$) close to the surface, as we have assumed, are quite consistent with small $\delta \mathbf{B}$, since, over a small depth d, *vortex lines are not field lines* in accordance with MS equations (Fig. 2).

C. The noise voltage

From Eq. (1), the noise voltage δV can be expressed as the sum of two terms we may refer to as the "ohmic" and "induced" terms, respectively. Taking a path (*asb*) lying in the bulk along a straight line parallel to the y axis (Fig. 1), we obtain

$$\delta V = \int_{asb} \delta E_y dy - \frac{\partial \delta \phi_{ms}}{\partial t} \ . \tag{16}$$

The two-step mechanism described above explains the occurrence of δE_y. But the question now arises, which of the two terms prevails in δV. In view of the smallness of the field noise, we expect that the induced term should be negligible in the low-frequency range of interest (0–2 kHz). This guess is clearly confirmed by explicit calculations in Sec. IV. Moreover, two obvious experimental facts corroborate the negligible contribution of $\delta \dot{\phi}_{ms}$. First, the low-frequency spectrum of the noise voltage *does not depend* on the spatial arrangement of the voltage leads. Furthermore, for any geometry of the pickup coils, the frequency dependence of the field-noise spectrum $S_{\phi\phi}$ coincides with that of the voltage-noise spectrum S_{VV}, see for example Fig. 7. A large term $\delta\dot{\phi}$ in V would introduce a significant component $f^2 S_{\phi\phi}$ in S_{VV}. Note that induced noise may become observable or relatively important either in the high-frequency tail of S_{VV} because of the factor f^2 ($f > 10^4$ Hz),[8] or in samples where, for independent reasons, the ohmic term itself is small. Concerning the latter point, our model clearly indicates which sample feature, apart from the defects, contribute to lower (or to enhance) voltage noise. For given noise sources $\delta \mathbf{i}_1$ and comparable δI_1, $\delta I_2 = -\delta I_1$ distributes throughout the cross section $t \times W$, so that small δE_y's should result from large cross sections and/or low flux-flow resitivities (pure metals). Conversely, large voltage noise is expected to be, and indeed is observed, in thin strips of alloys.

Disregarding the induced term and breaking up the ohmic term as stated in Eq. (3), we have

$$\delta V = \int_{ab} \delta E_y dy = \int B_z \delta v_{Lx} dy + \int v_{Lx} \delta B_z dy \ . \tag{17}$$

Here we have neglected small contributions, such as $v_{Lz}\delta B_x$ or $\delta v_{Lz} B_x$, due to vortices (and/or field lines) being slightly tilted in the bulk ($\nu_x, \delta\nu_x, \ldots$). Such terms are much smaller ($\lesssim 10^{-2}$) than the second term in Eq. (17), which, as we shall see, is far from being the dominant term in δV.

Making use of Eq. (15) we also can write, within the same accuracy,

$$\delta V = \int \rho_f \delta J_{2y} dy + \int J_{2y} \delta \rho_f dy \ . \tag{18}$$

In a large working range of temperatures and fields,[22] in particular in the experiments presented in this paper ($T/T_c \lesssim 0.3, B/B_{c2} \lesssim 0.6$), $\rho_f/\omega = \text{const}$ ($\rho_f \propto B$), so that $\delta\rho_f = \rho_f/\omega\, \delta\omega = \rho_f/\omega\, \delta B_z$. From Eq. (14), it is then readily seen that both terms of Eq. (18) identify with both terms of Eq. (17), respectively.

For the noise calculations of Sec. IV it will be convenient to assume that the sample is take as a "soft" piece $\Delta y = L$ from a long "hard" strip of width W. Both ends of the strip, where $\mathbf{v}_L \equiv 0, \mathbf{E} \equiv 0$, serve as equipotential leads. As far as any induced voltage $\dot{\phi}$ is negligible in comparison with the line integral of $\mathbf{E}$, the voltage V across such a sample, including its noise δV, is unambiguously defined and can be written as an integral (17) taken along *any* straight path $\Delta y = L$ lying in the bulk. This simple situation allows us to get rid of unimportant end effects ($\lesssim W/L$). Since the line integral of δE_y is independent of x and z, it will be useful to average Eq. (17) or (18) over the cross section, regardless of the negligibly small contributions of both surface layers. We thus obtain

$$\delta V = \frac{1}{Wt} \int\int\int \rho_f \delta J_{2y} dx\, dy\, dz + \frac{1}{Wt} \int\int\int v_{Lx} \delta B_z dx\, dy\, dz \ , \tag{19}$$

where the first term has been taken from Eq. (18) and the second from Eq. (17).

Assuming $v_{Lx}(y) \simeq \text{const}$, the second term in Eq. (19) may read $v_L/W \delta\phi_s$, where $\delta\phi_s$ is the field noise through the sample such as defined in Sec. II. Again, we may argue that, in contrast with shot-noise models, this noise term due to very small fluctuations δB_z of the magnetic field, should be negligible, except perhaps at very large v_L (or I_2). This conjecture is largely confirmed by experi-

ments (Sec. VI B).

Finally we are led to the conclusion that the voltage noise should essentially result from fluctuations of the bulk dissipative currents $\mathbf{J}_2$, which in turn result from fluctuations of surface currents $\mathbf{J}_1$, as suggested in Sec. III B.

The bulk vortex density $\omega \simeq \omega_z$ is uniform, and so is the flux-flow resistivity $\rho_f(\omega)$ for a normally homogeneous material. Thus, removing ρ_f from the first integral in Eq. (19), and ignoring the second term, δV simplifies to

$$\delta V \approx \frac{\rho_f}{Wt} \int \delta I_2 dy = R_f \langle \delta I_2 \rangle_y \ , \tag{20}$$

where $I_2 = I - I_1(y,t)$ is the bulk total current, such as defined above. $R_f = \rho_f L/Wt$ is the flux-flow resistance of the sample. Brackets with the subscript y indicate an average value along the sample length. According to our model, $I_1(y,t)$ can be interpreted as the instantaneous critical current at the cross section y. Its time average $\bar{I}_1(y)$ is the steady critical current. As the distribution of surface defects is hardly homogeneous in practice, different segments dy of the slab have different critical currents, scattered over a finite range, say from I' to I''. As easily checked by using a series of close voltage probes,[23] the voltage-current characteristic of the sample split up into a sum of elementary linear characteristics:

$$dV = \frac{\rho_f dy}{Wt}(I - \bar{I}_1) = v_{Lx}(y) B \, dy \ .$$

Hence, the curvature commonly observed at the foot of the overall characteristic (between I' and I''), and the linear part $V = R_f(I - I_c)$ at large currents ($I > I''$). The critical current I_c, usually obtained by extrapolating the linear part of the V-I curve, is nothing but $\langle \bar{I}_1 \rangle_y$. For the sake of the discussion, it will be useful to introduce a *fluctuating critical current* as

$$\langle I_1 \rangle_y = \langle \bar{I}_1 + \delta I_1 \rangle_y = I_c + \delta I_c \ , \tag{21}$$

in terms of which Eq. (20) can be rewritten as

$$\delta V \approx -R_f \delta I_c \ . \tag{22}$$

Now, to calculate $\delta\phi$ in any pickup coil, or in the measuring loop, as also $\delta I_c = \langle \delta I_1 \rangle$ in Eq. (21), we have to add some assumptions about the structure of the noise sources $\delta \mathbf{i}_1$. In Sec. IV, we shall describe surface currents $\mathbf{i}_1$ as a *2D homogeneous turbulent flow.*

IV. THE 2D TURBULENT FLOW MODEL

A. The current correlation tensor

For noise calculations being easily tractable, we must refer to a *standard* sample exhibiting a homogeneous distribution of surface defects. As a matter of fact, careful surface preparation enables us to approach uniform surface conditions, as will be borne out by the agreement between experimental results and quantitative predictions.

In a dc flux-flow experiment, surface currents are assumed to behave like a 2D *homogeneous* and *steady* turbulent flow. Note, however, a marked difference with more familiar problems of fluid dynamics, that is the noncontinuous character of the $\mathbf{i}_1$ field. Near the surface, supercurrents $\mathbf{i}_1$ can turn to bulk currents $\mathbf{J}_2$ ($\mathrm{div}\mathbf{i}_1 = \pm J_{2z} \neq 0$).

At any point $\mathbf{r}(x,y)$ of the sample surface, $\mathbf{i}_1$ may be divided into mean and fluctuating parts

$$\mathbf{i}_1 = i_c \hat{\mathbf{y}} + \mathbf{u}(\mathbf{r},t) \ . \tag{23}$$

Under standard conditions, $i_c = \mathrm{const}$, and the current space-time correlation tensor reads

$$\Gamma_{ik} = \overline{u_i(\mathbf{r},t) u_k(\mathbf{r}-\mathbf{R}, t-\tau)} = u^{*2} C_{ik}(\mathbf{R},\tau) \ , \tag{24}$$

where the bar indicates a time average, and u^* is the intensity of the turbulence ($u^{*2} = \overline{\mathbf{u}^2}$), so that $C_{ik}(0,0) \lesssim 1$. In a fully developed turbulence one should expect that $u^* \sim i_c$.

If surface defects disturb the moving vortex lattice over a small depth d, the resulting fluctuations $\delta \mathbf{i}_1 = \mathbf{u}$ should tend to remain localized, only giving rise to *short-range space correlations.* More precisely, we suppose that (for any τ) $C_{ik}(\mathbf{R},\tau)$ falls off more rapidly than $1/R^2$. In this respect, we emphasize that a continuity equation ($\mathrm{div}\mathbf{u} = 0$) would imply long-range longitudinal correlations ($C_{xx} \sim C_{yy} \sim 1/R$). Here, however, such a constraint is released thanks to the possible surface-to-volume transfer of currents.

It turns out that noise signals reported in this paper, including the longitudinal voltage, are all generated by the only component u_y of the noise sources. The corresponding auto and cross spectra can be merely expressed in terms of the y-y component of the correlation tensor. Denoting C_{yy} as $C(\mathbf{R},\tau)$ for short, and integrating over the XY plane, we obtain

$$\int\int C(\mathbf{R},\tau) dX \, dY = c^2 \chi(\tau) \ . \tag{25}$$

Taking $\chi(0) = 1$, Eq. (25) assigns a well-defined *length scale* c to the turbulence. Consistently with the continuum description of the vortex flow, and the idea of local fluctuations, we presume $a \ll c \ll W, L$. The Fourier transform $\Sigma(f)$ of $\chi(\tau)$ can be referred to as the normalized FFN spectrum. The frequency spectrum of all noise spectra will be dictated by $\Sigma(f)$.

B. Voltage- and field-noise spectra

Disregarding small and ill-defined transport currents along both edges of the slab, the critical-current fluctuation, such as given by Eq. (21), is

$$\delta I_c = \langle \delta I_1 \rangle_y = \frac{1}{L} \int\int u_y^+ dx \, dy + u_y^- dx \, dy \ , \tag{26}$$

where u^+ and u^- stand for the current fluctuations on the upper and lower faces, respectively. For brevity, the noise voltage (22) can be written as

$$\delta V = -R_f \delta I_c = -\frac{R_f}{L} \int\int_{\pm} u_y dx \, dy \ , \tag{27}$$

where the subscript $\pm$ will remind us to add both terms of Eq. (26). Since $\mathbf{u}^+$ and $\mathbf{u}^-$ fields are statistically in-

dependent, cross terms $\overline{u^+u^-}$ cancel systematically in calculating correlation functions. Therefore, contributions of both faces to any noise spectrum can be calculated separately and merely added.

To explore the magnetic-field noise, search coils have been designed to selectively detect the y component of the currents $\mathbf{i}_1$ and $\mathbf{J}_2$. This can be achieved ideally, by using rectangular loops, whose long edges (1) and (2) (of length $L' \gg L$) are parallel to the y direction, while being connected far apart from the sample. The magnetic flux $\delta\phi$ through one loop of such a coil, when expressed as the line integral of the fluctuating part $\delta\mathbf{A}$ of the vector potential, involves the only component δA_y:

$$\delta\phi = \int_{\text{wire(1)}} \delta A_y(\mathbf{r}')dy' - \int_{\text{wire(2)}} \delta A_y(\mathbf{r}')dy' \ . \tag{28}$$

Then, relating δA_y to its current sources, we have

$$\delta A_y = \frac{\mu_0}{4\pi}\int\int\int \frac{\delta J_{2y}}{r}dx\,dy\,dz + \frac{\mu_0}{4\pi}\int\int_{\pm}\frac{u_y}{r}dx\,dy \ , \tag{29}$$

where $r = |\mathbf{r}' - \mathbf{r}|$. Combining (28) and (29), and integrating over y', we obtain

$$\delta\phi = \frac{\mu_0}{2\pi}\int\int\int \mathbf{k}(\rho)\delta J_{2y}dx\,dy\,dz + \frac{\mu_0}{2\pi}\int\int_{\pm}\mathbf{k}(\rho)u_y dx\,dy \ , \tag{30}$$

where $\rho^2 = (x'-x)^2 + (z'-z)^2$, and $\mathbf{k}(x,z)$ is a dimensionless coupling coefficient, of order unity, given by

$$\mathbf{k}(\rho) = \ln\frac{\rho_2}{\rho_1} \quad (1 \text{ turn rectangular coil}) \ . \tag{31}$$

Here ρ_1 and ρ_2 are the cylindrical radial distances between the element of current at point $\mathbf{r}(x,y,z)$ and wires (1) and (2), respectively. As far as $\delta E_y \simeq \rho_f \delta J_{2y}$ (see the discussion of Sec. III C), the line integral of δJ_{2y} over y is independent of x and z ($=\delta V/\rho_f$). Moreover, $\mathbf{k}$ does not depend on y, so that the first integral in Eq. (30) can be factorized as

$$\int\int \mathbf{k}(\rho)dx\,dz \int \delta J_{2y}dy = \langle \mathbf{k}(\rho)\rangle_{xz} L \langle \delta I_2 \rangle_y \ . \tag{32}$$

Note that $\langle \mathbf{k}(\rho)\rangle_{xz}$, the average value of $\mathbf{k}$ over the cross section $W \times t$, is a constant. Making use of Eqs. (21) and (27), both integrals in Eq. (30) can be cast into the compact form:

$$\delta\phi = \frac{\mu_0}{2\pi}\int\int_{\pm} K u_y dx\,dy = \frac{\mu_0 L}{2\pi}\delta I_k \ , \qquad K = \mathbf{k}(x,z) - \langle \mathbf{k} \rangle_{xz} \ . \tag{33}$$

In Eq. (33) δI_k appears as a current noise which, like δI_c, is calculated from the noise sources, except for weighting u_y by the coupling coefficient K. If $K \sim 1$ (Fig. 4), $\delta I_{\mathbf{k}} \sim \delta I_c$, and from Eqs. (27) and (33), we expect that $\delta\phi/\delta V \sim \mu_0 L/2\pi R_f$ (typically 10^{-5} s) for a single loop.

Two kinds of coils were used in the present work, which we shall refer to as C_z [Fig. 3(a)] and C_x [Fig. 3(b)]. They consist of rectangular loops $L' \times W'$ in xy planes, or $L' \times t'$ in yz planes, respectively. Though overlapping the sample, they of course have a finite length L'. Whence the above result must be corrected in two respects. First, integrals (28) must be taken over the finite interval $(-L'/2, L'/2)$. On the other hand, we have to add the line integral of δA_x (resp. δA_z) over the wires parallel to the x (respectively, z) direction, which result from currents δJ_{2x} and u_x (respectively, δJ_{2z}). By relying on simple and model-consistent assumptions about the noisy currents ($u_x \sim u_y, \delta J_{2z} \sim \text{div}\mathbf{u}$), and following the same procedure, an overestimate of the correcting terms in $\delta\phi$ can be calculated, though at the cost of some tedious algebra. Thus we have ascertained that these corrections, for $L' \sim 2L$, did not affect the theoretical spectra significantly ($\lesssim 3\%$), seeing that the statistical error in measuring them is bout 5%. Moreover, the good agreement between the measured spectra (S_{VV} and $S_{\Phi\Phi}$) and quantitative predictions from Eqs. (27) and (33), will support both the correctness of the model, and the validity of the infinite-coil approximation.

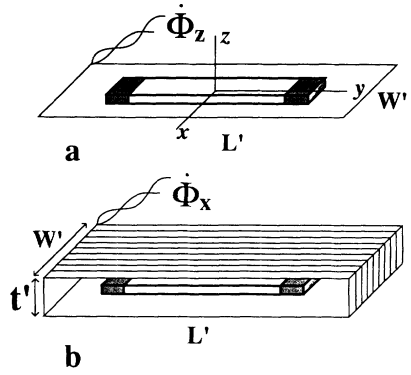

FIG. 3. Two pickup coil configurations were used to measure the field noise around the sample: (a) A flat coil (10 turns) in the sample plane, labeled C_z in the text. It roughly measures the fluctuations of the sample flux ϕ_s, and is best suited to compare our predictions with those of shot-noise models; (b) A flat rectangular solenoid labeled C_x which is sensitive to the x component of the field noise. It was designed to reveal 3D effects in a thick slab. For strictly 2D motions of vortices, ϕ_x would be zero.

Finally, we find that the voltage noise δV as well as $\delta\phi$ in Eq. (33), and, by superposition, the flux noise $\delta\Phi_x$ or $\delta\Phi_z = \sum\delta\phi_i$ through the N turns of a C_x or a C_z coil can be written in the same general form as function of the noise sources u_y:

$$A = \int\int_{\pm}\alpha(x,z)u_y dx\,dy \ , \tag{34}$$

where $\alpha = -R_f/L = \text{const}$ for $A = \delta V$ [from Eq. (27)], and $\alpha(x,z) = \mu_0/2\pi\sum K_i$ for $A = \delta\Phi$. Auto and cross spectra of quantities expressed in the form (34) are derived at in Appendix B. From (B6) we immediately obtain the power spectrum of the voltage noise:

$$S_{VV}(f) = 2R_f^2\frac{W}{L}u^{*2}c^2\Sigma(f) \ . \tag{35}$$

The factor 2 here accounts for the added effects of both faces.

The flat coil C_z encircling the slab in its plane [Fig. 3(a)] was designed to observe the fluctuations of the sam-

ple flux ϕ_s, with the purpose, in particular, of comparing our predictions with those of the shot-noise model (see Sec. II). It is made of $N\sim 10$ rectangular turns, the sensing wires of which lie at $x'=\pm W'/2, z'\simeq 0$. For $W'\gtrsim 1.3W$, the coupling coefficient K_i (and derived quantities; see for instance, Fig. 4) is practically independent of z and z' ($z=\pm t/2$, $z'\lesssim t$), so that $\delta\Phi_z\simeq N\delta\phi$, where $\delta\phi$ may be calculated in the limit $z=z'=0$, $t\to 0$. If the coil C_z and the sample are carefully centered, by symmetry

$$\langle K\rangle_x=\langle k\rangle_x=0 .$$

Substituting $\alpha=-R_f/L=\text{const}$ and $\beta=(\mu_0/2\pi)K$ in expression (B5) for the correlation coefficient $\sigma_{V\phi}$, we obtain the important result that no correlation should exist between δV and $\delta\Phi_z$, in contrast with the shot-noise result (C5),

$$S_{V\Phi}=0 \quad \text{and} \quad \gamma^2_{V\phi}=0 \quad (\text{coil } C_z, \Phi=\Phi_z) . \tag{36}$$

Likewise, the autocorrelation coefficient $\sigma_{\phi\phi}$ is expressed in terms of

$$\langle K^2\rangle_x=\langle k^2\rangle_x=K^{\dagger 2} .$$

As remarked above, $K^\dagger(z-z')\simeq\text{const}\sim 1$, for $W'\gtrsim 1.3W$ (see Fig. 4), so that $\sigma_{\phi\phi}=2(\mu_0 K^\dagger/2\pi)^2$. Then, from Eqs. (B6) and (35), we obtain

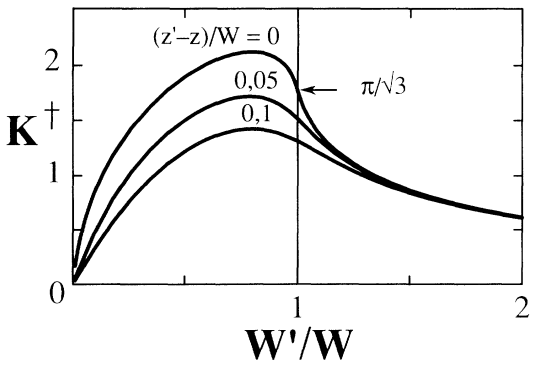

FIG. 4. A coupling coefficient K has been introduced in Eq. (33) to calculate the magnetic-flux noise $\delta\phi$ in any large rectangular loop ($L'\gtrsim L$). The field-noise spectrum $S_{\phi\phi}$ depends on the loop geometry through the autocorrelation coefficient $\sigma_{\phi\phi}$. This is given by Eq. (B5) as the sum of two terms, which represent the variances $K^{\dagger 2}$ (x average) of K, as calculated on both faces $z=\pm t/2$ of the sample. Here the rms value $K^\dagger$, related to a rectangular loop $W'\times L'$ in a plane z' [one turn of the coil C_z in Fig. 3(a)], is plotted vs W'/W, for various values of $z'-z$. The coil used in previous measurements (Ref. 20) was wound close to the sample edges ($W'\simeq W$), and Eq. (7) of Ref. 20 was obtained by assuming $W'=W$, $t=0$, $z'=z$, and letting $K^\dagger=\pi/\sqrt{3}$. As appears from the figure, at $W'=W$, $K^\dagger$ may take somewhat different values depending which sample face or coil turn is considered ($t\sim z'-z\sim 0.1W$). A better quantitative prediction can be gained by taking $W'\gtrsim 1.3W$, since there $K^\dagger$ becomes practically independent of the coil and sample thicknesses. This circumstance has determined the width W' of the coil C_z.

$$S_{\phi\phi}=2\left[\frac{\mu_0 L}{2\pi}\right]^2 K^{\dagger 2}\frac{W}{L}u^{*2}c^2\Sigma(f) ,$$

$$(\text{coil } C_z,\ \phi=\Phi_z \text{ per turn}) \tag{37}$$

$$\left[\frac{S_{\phi\phi}}{S_{VV}}\right]^{1/2}=\frac{\mu_0 L}{2\pi R_f}K^\dagger=\text{const}(f) .$$

The latter equation is put in the same form as Eq. (35) by introducing the "sample inductance" $\mu_0 L/2\pi$.

We are now in a position to estimate the contribution to S_{VV} of the second term in Eq. (19), viz. $v_L/W\delta\phi_s$, which has been disregarded deliberately in deriving Eq. (35). From Eqs. (36) and (37), the normalized correction to Eq. (35), $(v_L/W\ \mu_0 L K^\dagger/2\pi R_f)^2\sim 10^{-6}$, is proved completely negligible.

The coil C_x is a rectangular solenoid whose axis coincides with the x axis [length $W'\geq 3W$, cross section $L'\times t'$; Fig. 3(b)]. It picks up the x component of the field noise. One easily realizes that $\delta\Phi_x$ would be zero for strictly 2D vortex motions: Any current field in this case may be regarded as resulting from the superposition of current loops lying in xy planes, with no exchange between planes; if the slab is located at the center of the solenoid, as shown in Fig. 3(b), there is no coupling between these loops and C_x. For the same reason, $\delta\Phi_x\to 0$ when $t\to 0$, irrespective of the model involved. Therefore, provided that thick slabs ($t\sim 0.1W$) are used, the C_x-coil geometry will be suitable to reveal 3D effects in the vortex distribution, in particular the surface-to-volume fluctuations $\delta I_1=-\delta I_2$ as implied by our model. Φ_x can be written in the form (B1) with the weighting factor

$$\beta(x,z)=\mu_0/2\pi\sum_1^N K_i=\mu_0/2\pi N\langle K\rangle_{x'} . \tag{38}$$

In calculating $\langle K\rangle_{x'}$ in Eq. (38), we may ignore second-order terms, as x^2 and z^2, without loss of accuracy ($\lesssim 1\%$ for $W'=3W$). We thus obtain an expression for β linear in z:

$$\beta(z)=\frac{\mu_0 N}{2\pi}\frac{4z}{W'}\arctan\left[\frac{W'}{t'}\right]\leq\mu_0 N\frac{z}{W'} . \tag{39}$$

Taking $N\sim 100$, $W'\sim 1$ cm, $z'\sim 0.1$ mm, the β factor is comparable with that of a ten turns C_z coil ($\beta\sim\mu_0$). On writing $\beta=b_1 z$, b_1 is nothing but the virtual self-field produced at $x=z=0$ by a unit current through the coil C_x. As far as this self field is uniform near the center of the solenoid, the above result will not be affected by any slight shift of C_x parallel to the z axis.

According to Eq.(39), β is independent of x so that $\langle\beta\rangle_x=\beta$ and takes opposite values on the two faces:

$$\beta(t/2)=\beta_+=-\beta_-=\left[\frac{\mu_0 N}{2\pi}\right]\frac{2t}{W'}\arctan\left[\frac{W'}{t'}\right]$$

$$=\left[\frac{\mu_0 N}{2\pi}\right]K' . \tag{40}$$

The so-defined coefficient K' is typically of the order of 0.1. Using Eq. (B5), the correlation coefficients $\sigma_{V\Phi}$ and $\sigma_{\Phi\Phi}$ simplify to

$$\sigma_{V\Phi}=-\frac{R_f}{L}(\beta_+ +\beta_-)=0 ,$$
$$\sigma_{\Phi\Phi}=2\beta_+^2=2\beta_-^2 , \tag{41}$$

whence we obtain the spectra

$$S_{V\Phi}=0 , \text{ or } \gamma_{V\Phi}^2=0 , \quad (\text{coil } C_x,\ \Phi=\Phi_x) \tag{42}$$
$$S_{\Phi\Phi}=2\left[\frac{N\mu_0 L}{2\pi}\right]^2 K'^2\frac{W}{L}u^{*2}c^2\Sigma(f) .$$

Letting $\phi=\Phi_x/N$ as the mean flux per turn, and comparing with Eq. (35), we obtain, like Eq. (37)

$$\left[\frac{S_{\phi\phi}}{S_{VV}}\right]^{1/2}=\frac{\mu_0 L}{2\pi R_f}K'=\text{const}(f)$$
$$(\text{coil } C_x,\ \phi=\Phi_x \text{ per turn}) . \tag{43}$$

Again, like V and Φ_z, there should be *no correlation* between V and Φ_x. Nevertheless, by using different surface treatments on purpose, we can introduce a strong asymmetry between the two faces, and, as we now show, this might make V and Φ_x fully coherent in an extreme case. Suppose for example, that the lower face $z=-t/2$ be markedly softer; as noise spectra vary as u^{*2}, and $\mathbf{u}^*\sim i_c$, the FFN would be essentially generated on the upper face. Thus, from Eqs. (B1) and (27), we should have

$$\delta\Phi_x(t)=\beta_+\int\int_+ u_y dx\,dy=\beta_+ L\delta I_c(t)=-\frac{\beta_+ L}{R_f}\delta V(t) , \tag{44}$$

meaning that $\delta\Phi_x$ and δV *should be proportional.* While the relative amplitude (43) of both noises has not changed, $\gamma_{V\Phi}^2=1$ instead of zero when both faces are equally active.

V. EXPERIMENTAL SETUP

Noise measurements reported in this work have been performed on a series of Pb-In slabs, with approximate dimensions $L=30$–50 mm, $W=4$–10 mm, and $t=0.2$–0.5 mm. In Sec. VI B, we also mention some preliminary but significant results obtained with Pb-In and pure Nb square rods (4×4 mm^2 cross section).

Homogeneous lead-indium alloys are easily prepared from pure metals,[11] and extensive measurements in the literature yield reliable values of their H_{c2}, κ, and ρ_n (normal resistivity).[24] Our procedure is similar to that followed by Thompson and Joiner.[11] The starting materials (6*N* lead and 5*N*5 indium) were melted in a Pyrex tube under purified argon ($\sim10^{-4}$ mm Hg). After a 40 h period at about 100 K above the melting temperature, the tube was quenched at the room temperature. Optional annealing of the cast ingot, for two weeks within about 10 K of the solidus point, improves the bulk homogeneity of the solid solution. The composition of all samples was Pb-In 17.5 at. %. The corresponding parameters are $T_c=6.95$ K, $B_{c2}(0)=5400$ G, $\kappa\simeq3.5$, and $\rho_n=10.5$ $\mu\Omega$ cm.

Thick slabs were spark cut directly from the ingot, and then rolled and/or pressed to the final desired thickness. The best approach to standard surface conditions, such as defined in Sec. IV A, were obtained by pressing a thick slab between glass microscope slides with a 1-ton hydraulic press. Pressed samples exhibited a mirrorlike finish, a good parallelism of the faces, and yet relatively large critical currents. Images by scanning tunneling microscopy revealed a very rugged surface on the scale of the vortex spacing, consistent with the MS model for critical currents. Nickelling was used to reduce critical currents when necessary; apparently, electroplating acts as a uniform smoothing of the surface.

We have to ascertain that a part of the investigated noise (δV or $\delta\dot{\Phi}$) is not due to spurious fluctuations of the state parameters, namely T, B_0, I. Indeed, since $\varepsilon(B,T)$, and then i_c, are temperature dependent, any δT in the mixed state will result in fluctuations δI_c, irrespective of the irregularities of the vortex motion. In a previous work,[25] we have shown that this possible source of noise is avoided, in spite of large power inputs ($VI\lesssim250$ mW), by immersing the sample in a superfluid helium bath far enough from the λ point ($T\sim1.8$ K).

More importantly, while measuring $\delta\Phi$'s, the applied magnetic field itself must be free from noise. The residual field noise of the electromagnet ($\delta B_0\sim1$ mG/Hz$^{1/2}$ in the 0–20 Hz range), as well as external magnetic perturbations are efficiently shielded by using a 1-cm-thick high-conductivity copper box.[11] The applied current $I=0$–40 A was delivered by a bank of 6 V-450 A h storage batteries. It could be varied stepwise by means of a set of resistors (60 W, oil-cooled) connected in series with the sample.

While it is relatively easy to detect the voltage noise δV (at least in alloys), measuring FFN induced voltages $\delta\dot{\Phi}$, so small as predicted in Sec. IV, is a real difficulty. These would be overlapped by any disturbances of the applied field $\delta B_0\sim10$ μG/Hz$^{1/2}$. Even when screening the temporal fluctuations $\delta B_0(t)$ by means of a copper box, the slightest vibration of a pickup coil immersed in a field $B_0\sim0.1$–1 T can result in strong fluctuations δB_x or δB_y obscuring broad bands of the low-frequency FFN spectrum. In spite of precautions for securing the least part of the sample and coils assembly, microphonic effects, due to liquid-nitrogen bubbling, were still disturbing for the purpose of this work. Decisive improvement was achieved by merely sealing the nitrogen jacket. Letting the pressure rise from 0.2 to 1.5 bar, ensured us 1-h quiet runs.

In order to obtain low noise figures of the detection system, signals δV and $\delta\dot{\Phi}$ were fed to two helium-cooled setup transformers having a turns ratio of 1:200. The toroidal strip-wound cores are made of an amorphous Co-based alloy, whose magnetic properties are preserved at very low temperatures. Each transformer is enclosed

in an ellipsoidal lead capsule. When placed outside the high-field region, the capsules act as zero-field chambers. Whereas mechanical vibrations mainly interfere with the primary signals, the secondary high-impedance circuit (20 kΩ) is highly sensitive to statics and triboelectric effects. The latter are due to thermal strains in transmission cables leaving the helium vessel. In this respect, we found it essential to use low noise coaxial cables: application of a carbon layer on the surface of the insulator (PTFE) allows charges to flow away. After amplification (10^3–10^4) with nanovolt preamplifiers, the signals were processed by a two-channel spectrum analyzer (Solartron 1200), which provides a wide range of analysis and display facilities of both correlation functions and spectra. The upper and lower cutoff frequencies of the entire system were restricted by the transformers, depending on the primary input impedance. For instance, in noise voltage measurements, a 0.5-Ω resistor was connected in series in the primary circuit in order to limit diverted dc currents from the sample (~1 mΩ). Under such conditions, we obtained a flat response (±5%) in the range 10 Hz–10 kHz.

With these precautions, we were able to detect flux-flow noise signals δV or $\delta\dot{\Phi}$ as small as 10 pV/Hz$^{1/2}$. Such a background voltage is comparable with the thermal Johnson noise of a 1-Ω resistor at 2 K. An even better resolution is achieved in cross-correlation measurements, since these remove the incoherent thermal and electronic noises of the two channels. When expressed in terms of $\delta\phi$ ($\delta\Phi$ per turn), the resolution in the mid region of the FFN spectrum (~1 kHz) may be as low as $10^{-2}\varphi_0/\mathrm{Hz}^{1/2}$ per turn for a 100 turn coil. We emphasize that, in a high magnetic field environment, such a conventional system may well stand comparison with a superconducting quantum interference device system.[9] By using two pickup coils and measuring cross spectra, we have checked the applied field and current stability in the working frequency range. On setting $I=0$ at $B_0 \lesssim 0.5$ T and $I \lesssim 40$ A at $B_0=0$, respectively, we obtain

$$\delta I \lesssim 10\ \mathrm{nA/Hz^{1/2}}\ ;\quad \delta B_0 \lesssim 10\ \mathrm{nG/Hz^{1/2}}\ .$$

VI. EXPERIMENTAL RESULTS

A. Noise voltage in the flux-flow regime

In this paper, we are concerned with the properties of the FFN in full flux-flow regime, when the whole vortex lattice has been set in motion ($I > I''$, see Sec. III C). For various practical reasons (higher noise level, low input power), earlier measurements of the voltage noise were essentially confined to the curved region of the V-I characteristics ($I' < I \lesssim I''$). So the authors failed to notice simple and regular features of the FFN, that only appear along the linear part of the V-I curve. Figure 5 shows δV spectra obtained for increasing values of the applied current, form $I \gtrsim I'$ up to $I \approx 2I_c$. These clearly reveal two noise regimes corresponding to currents either smaller or larger than I'' (Figs. 5 and 6).

Using a 0–10-kHz bandwidth, the signal analyzer provides an accurate estimate of the rms value of the noise voltage δV^* (noise intensity):

$$\delta V^{*2} = C_{VV}(0) = \int S_{VV}(f)df\ . \tag{45}$$

Errors due to missing the high-frequency tail of $S_{VV}(f)$, as also to the low-frequency cutoff ($\lesssim 10$ Hz) of the transformers, are negligible. A transformer was specially designed to explore the very low-frequency range of the noise spectrum, down to 1 Hz. Thus, we made sure of the linear frequency dependence of $S_{VV}(f)$ at the zero-frequency limit; in particular, no singular behavior, such as a $1/f$ dependence, was observed.

Two features typical of the flux-flow regime should be emphasized. First, note that, above I'', the noise level is nearly constant (Fig. 6). More strikingly, the normalized spectrum $\Sigma(f)$ *is stationary*. In other words, plots of spectra (d), (e), (f) in Fig. 5(b) can be superimposed (within statistical uncertainty) by mere rescaling. Since $\Sigma(f)$ is independent of I (or v_L) and retains the same general shape at different fields in different samples, FFN voltage is well characterized by its intensity δV^*. For definiteness, we shall refer to the value $\delta V^*(0)$ obtained by extrapolating the flux-flow line $\delta V^*(I)$ at $I = I_c$ (or

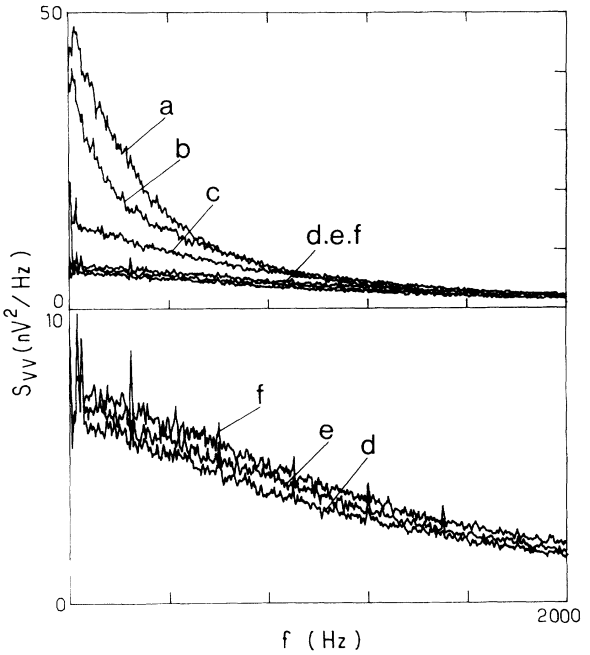

FIG. 5. The low-frequency auto power spectrum of the noise voltage $S_{VV}(f)$ is measured at $T = 1.88$ K, $B = 1000$ G, for various values of the applied current along the V-I curve as shown in Fig. 6. The sample is a Pb-In 10.5 wt. %, $L = 40$ mm, $W = 6.9$ mm, $t = 0.19$ mm. Here, $S_{VV}(f)$ is displayed in linear format with a 4-Hz resolution (2-kHz frequency span). Under these conditions, after a 1–2 min run, the statistical uncertainty is about $10\% \sim 1/\sqrt{N}$, where $N \sim 100$ is the number of instantaneous measurements averaged. Spectral labeled $a, b, \ldots, f$ refer to increasing values of the current such as indicted in Fig. 6. When the flux-flow regime is achieved, i.e., along the linear part of the V-I curve (d-e-f), the normalized spectrum has become stationary, while its amplitude is nearly constant. Note that, from d to f, the line velocity v_L was doubled.

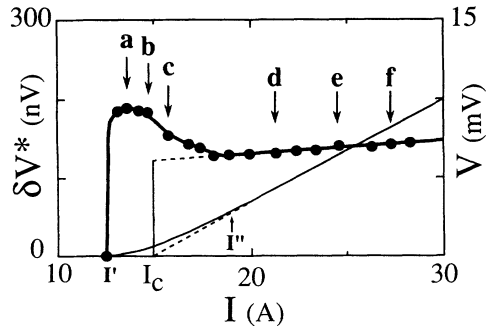

FIG. 6. The dc voltage and the rms value of the voltage noise δV^* as a function of the applied current. The full line is a guide for the eye. Experimental conditions (T,B, sample) are those stated in caption of Fig. 5. δV^* is obtained on integrating $S_{VV}(f)$ over the frequency range 0–10 kHz. The arrows mark the operating points, $a,b,\ldots f$, of Fig. 5. The noise behavior undergoes a marked change at the beginning of the linear part of the V-I curve ($I=I''$ as defined in Sec. III C). According to the exact transverse position of both voltage contacts **a** and **b**, either a slight increase or decrease of δV^* was observed in the flux-flow regime. This should be ascribed to unimportant end effects ($\sim W/L$), (Ref. 17) which have been systematically ignored in our calculations. Nor is the model of Sec. IV relevant to the intricate noise data observed in the curved region of the V-I curve. Thus, the extrapolated value at $I=I_c$ ($\langle v_L \rangle_y = 0$), denoted as $\delta V^*(0)$ in the text, may be taken as the representative amplitude of the flux-flow noise voltage.

$V=0$, or $\langle v_{Lx} \rangle_y = 0$) as shown in Fig. 6.

A long strip and well-separated contacts (a and b) ($ab = L \gg W$) imitates the ideal situation of equipotential ends such as assumed in calculations of Sec. IV. This means a strong correlation between voltages V_1 and V_2, taken from two pairs of opposite contacts a_1b_1 and a_2b_2 along the edges of the strip. To the eye, instantaneous displays of both time wave forms $\delta V_1(t)$ and $\delta V_2(t)$ do coincide. More precisely, measurements of the normalized cross correlation γ_{12} [see Eq. (B7)] bring out small differences between δV_1 and δV_2. For instance, taking $L = 10W = 40$ mm, we found typically $|\gamma_{12}| = 0.95$, while its phase does not exceed 5° over the useful band width. In contrast, there is no detectable longitudinal correlation, so that noise intensities add for adjacent contact pairs (S_{VV} or $\delta V^{*2} \propto L$). Small differences between δV_1 and δV_2 are consistent with the observation of noisy transverse voltages across a_1a_2 and b_1b_2. There is no dc Hall effect in the sense that $v_{Ly} = 0$, but Hall noise does exist. It reveals fluctuations δv_{Ly}, which appears to be of the same order of magnitude as those of v_{Lx}.

As shown by our experimental results as a whole, a good standard homogeneity of the surface state ensures a fair homogeneity of the turbulence. But, as discussed in Sec. III C, surface conditions are never so perfect as to achieve the uniformity of the critical current $\bar{I}_1(y)$, and hence, that of the dc line velocity $v_{Lx}(y)$. In consequence, we cannot hope to observe something like a transition to turbulence by letting $v_L \to 0$ throughout the sample. Nevertheless, as a regular FFN regime starts at $I=I''$ (Fig. 6), it is plausible that the surface-current flow be fully turbulent at the very first vortex motion. At $I > I''$, $v_{Lx}(y)$ (like $I - \bar{I}_1$; see Sec. III C) increases, but keeps different values in different segments dy of the sample. The perfect stability of the FFN spectrum under these conditions, $v_L(y)$ and $v_L(I)$, bears out that changes in v_L do not affect the structure of the turbulence.

B. Field noise versus voltage noise

The induced emf $\dot{\Phi}$ across the search coil (C_x or C_z, Fig. 3) is processed after preamplification. Thus, by using the input integration facility of the signal analyzer, all spectra are divided by $(2\pi f)^2$, so that the relative contribution of the spurious electronic noise is enhanced at low frequencies. On the other hand, due to the inductance of the pickup coil, an additional resistor must be inserted in the primary circuit to flatten the transformer response, at the cost of a decrease of the upper cutoff. In practice, we ascertained that $S_{\Phi\Phi}$ be accurately measured within the restricted band 600–1600 Hz. This range is large enough, however, to check and compare the frequency behavior of various spectra.

Let us first state the main experimental facts without referring to any interpretation. As an example, Fig. 7 shows an overlay view of simultaneous recordings of S_{VV} and $S_{\Phi\Phi}$ (from coil C_x). Both traces are superimposed, again within statistical uncertainty, by mere adjusting the scales. Such an exact coincidence was observed for whichever sample and coil, at any fields and currents in the flux-flow regime. As a first clear result, low-frequency voltage and field noises *do have* the same normalized spectrum $\Sigma(f)$. As discussed in Sec. III C, this justifies neglecting the induced term $\dot{\phi}_{ms}$ in δV. A rms amplitude of the field noise $\delta\Phi^*$ can thus be deduced from δV^*, on identifying $(\delta\Phi^*/\delta V^*)^2$ with the spectrum ratio $S_{\Phi\Phi}/S_{VV}$ as measured in the selected frequency span. Typically, at $B_0 \sim 1000$ G, $\delta\phi_x^* \sim 100\varphi_0$/turn, and $\delta\phi_z^* \sim 1000\varphi_0$/turn, to be compared with the sample flux $\phi_s = B_0 WL \sim \phi_z \sim 10^{10}\varphi_0$. These orders of magnitude are consistent with the conclusion that $\dot{\phi}_{ms} \ll \delta V$, and also confirms the negligible part in δV of terms such as $v_L \delta B_z$ [see Eq. (17) and comments]. It should also be noted that, whereas slight variations of δV^* are observed along the linear part of the V-I curve (Fig. 6), the amplitude ratio $\delta\Phi^*/\delta V^*$ is found to be a constant within experimental accuracy. But, on the other hand, $\delta\Phi^*/\delta V^*$ is strongly field dependent, as illustrated in Fig. 8. Concerning cross correlations, the coherence function $\gamma^2_{V\Phi}$ was found to be very small in the best samples: $0 \lesssim \gamma^2 \lesssim 0.05$, for both coils C_x and C_z, depending on the applied magnetic field. In fact, $S_{V\Phi}$ turns out to be very sensitive to slight departures from standard surface conditions (Sec. V). As a proof, a surface inhomogeneity was introduced by nickelling one face of the slab. As a result, I_c and δV^* were reduced, but the ratio $\delta\Phi_x^*/\delta V^*$ was unchanged, while $\gamma^2_{V\Phi}$ for C_x significantly increased: $0.1 \lesssim \gamma^2 \lesssim 0.3$. We return to this point below.

It is clear that theoretical predictions of a shot-noise model are totally at variance with our experimental results. According to a shot-noise model (i) the frequency dependence of S_{VV} and $S_{\Phi\Phi}$, depending on the spatial arrangement of voltage leads and coils, are different in gen-

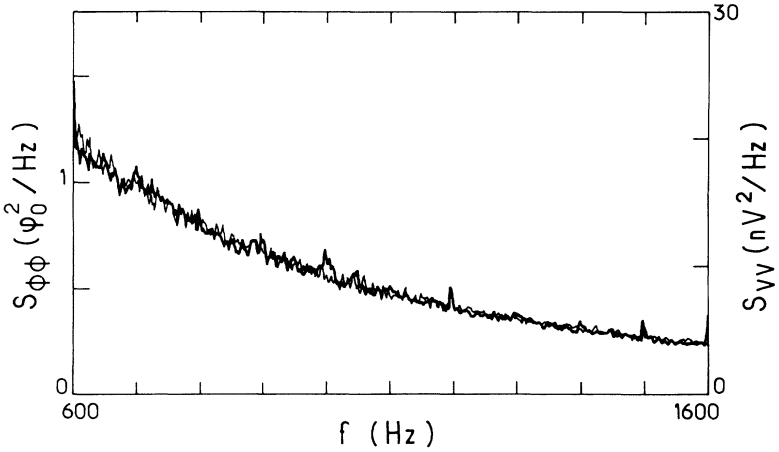

FIG. 7. The field-noise spectrum $S_{\phi\phi}$ for the C_x coil, where $\phi=\Phi_x/N$ (Φ_x per turn; $N=72$), and the voltage noise S_{VV}, are recorded simultaneously in the frequency band 600–1600 Hz, at $T=1.8$ K, $B=1500$ G, $I=20.8$ A. By setting the appropriate scaling factor, both traces intermingle, meaning that normalized spectra coincide within statistical uncertainty ($\sim 1/\sqrt{N}\sim 4$–5%; $N\sim 500$; recording time ~ 3 min). Note the minuteness of the field noise ($\delta\phi^* \lesssim 100\varphi_0$ per turn). Sample dimensions $L=38$ mm, $W=4.8$ mm, $t=0.34$ mm. C_x coil dimensions $L'=80$ mm, $W'=15$ mm, $t'=6$ mm.

eral; (ii) the relative amplitude $\delta\phi_z/\delta V$ decreases with increasing currents, as $1/v_L$ [Eq. (6)]; (iii) expected $\delta\phi_z^* \simeq \delta\phi_s^* \sim 10^5$–$10^6\varphi_0$ lead to spectrum amplitudes much larger than observed, by a factor 10^4–10^6; (iv) as shown in Appendix C, δV and $\delta\Phi$ are fully coherent ($\gamma^2_{V\Phi}=1$).

By contrast, the model developed in Sec. IV has the immediate virtue of accounting for the above experimental facts qualitatively and coherently. The most powerful result, however, consists in predicting values of $\delta\Phi^*/\delta V^*$ only in terms of known parameters. In all expressions of noise spectra derived in Sec. IV B, u^*c appears as the one adjustable parameter. But for a given voltage noise, in a given sample, we are able to calculate auto and cross correlations of the field noise for a variety of coils. Collecting Eqs. (35), (37), and (43), and integrating spectra, we have

$$\delta V^* = R_f \delta I_c^* = R_f \left[\frac{2W}{L}\right]^{1/2} u^* c \ , \tag{46}$$

$$\frac{1}{K^\dagger}\frac{\delta\phi_z^*}{\delta V^*} = \frac{1}{K'}\frac{\delta\phi_x^*}{\delta V^*} = \frac{\mu_0 L}{2\pi R_f} \ , \tag{47}$$

where δI_c^* is the rms fluctuation of the critical current; ϕ stands for the magnetic flux per turn, and $K^\dagger$ and K' are two dimensionless geometrical factors. δV^*, $\delta\Phi_z^*$, and $\delta\Phi_x^*$ have been investigated for values of the magnetic field ranging from 500 to 2500 G. In this range, the flux-flow resistivity ρ_f, then R_f, increases with increasing field by a factor of about 5. At lower fields, I_c becomes too large. At higher fields, δV^* and $\delta\Phi^*$ all the more, begins to fall off; on the other hand, coils (especially C_x) are more sensitive to residual microphonics. The remarkable quantitative agreement with predicted values of $\delta\Phi^*/\delta V^*$ from Eq. (47), for two different coil geometries, is quite convincing (Fig. 8).

Concerning $\delta\Phi_x$, we wish to make a point. As remarked in Sec. IV B, $\delta\Phi_x$ should be zero for strictly 2D vortex motions, and $\delta\Phi_x \to 0$ when $t\to 0$ ($K' \propto t$). Indeed, the coil C_x was just designed to reveal 3D fluctuations, over the thickness t, of the current and vortex distribution. Disregarding detailed algebra of the model, but dwelling on the smallness of $\delta\Phi_x$ and the absence of correlation between $\delta\Phi_x$ and δV, one might argue that such 3D effects are irrelevant to the noise voltage mechanism. In fact, $S_{\Phi V}=0$ is a mathematical circumstance due to the symmetric role of both faces of the sample. In Sec. IV B, we have shown that a single turbulent plane would generate a fully coherent voltage noise ($\gamma^2=1$). Of course, we could not get a face clear of surface defects and noise sources, but a partial correlation was restored, as seen above, by plating one face. For instance, if $u^* \sim i_c$ is reduced on this face by a factor of 2 [$\Gamma_+ = 4\Gamma_-$ in Eq. (B3)], a straightforward calculation gives $\gamma_{\Phi V}=\frac{3}{5}$ or $\gamma^2=0.36$.

Earlier noise measurements had been performed,[17] using Pb-In and Nb square rods of $W\times W = 4\times 4$ mm^2 cross section. Two small pickup coils, linking noisy fluxes $\delta\Phi_1$ and $\delta\Phi_2$, were located at the center of two opposite faces as shown in Fig. 9. This experimental arrangement was not so suitable for precise analytical calculations, but the model of Sec. IV successfully predicted

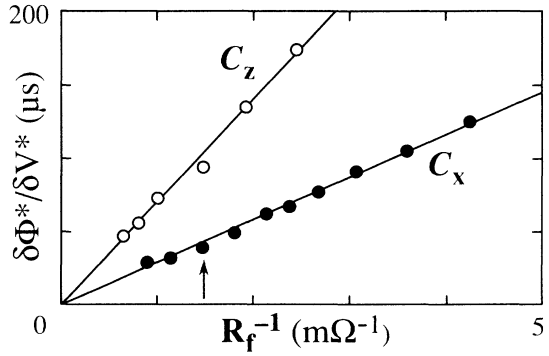

FIG. 8. The ratio $\delta\Phi^*/\delta V^*$ of the rms amplitudes of field and voltage noises, as a function of $1/R_f$. R_f is the field-dependent flux-flow resistance ($500 \le B \le 2500$ G). The solid straight lines are theoretical curves. Their slopes are calculated from Eq. (47) without adjustable parameters. (●): Coil C_x (72 turns). Sample and coil dimensions, see caption of Fig. 7. The arrow marks the point deduced from data in Fig. 7. (○): Coil C_z (10 turns). Sample dimensions $L=40$ mm, $W=3.9$ mm, $t=0.38$ mm. Coil dimensions: $L'=65$ mm, $W'=6$ mm.

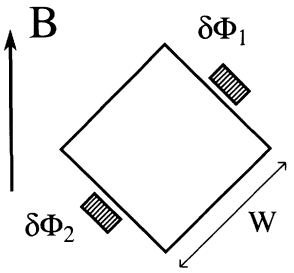

FIG. 9. Small pickup coils (0.5 mm×1 mm section, 15 mm length) were arranged around PbIn and Nb square rods ($W\times W=4\times4$ mm) close to the surface, so as to demonstrate the surface-volume (or I_1-I_2) fluctuations in the distribution of the transport current, and the statistical independence of the surface-current fluctuations, as discussed at the end of Sec. VI C.

auto and cross power spectra of δV, $\delta\Phi_1$, and $\delta\Phi_2$.[17] Some results obtained with this geometry are worth mentioning, as they complete our argument. There is practically no correlation between $\delta\Phi_1$ and $\delta\Phi_2$: $\gamma^2=2.5\times10^{-3}\pm2\times10^{-3}$, after 1–2 h averaging time. This brings out that current fluctuations $\delta\mathbf{J}$ (the sources of the field noise) are, for the most part, superficial and statistically independent. A rough estimate of the coherence function, that would result from a bulk distribution of incoherent $\delta\mathbf{J}$'s, yields $\gamma^2\sim0.1$ instead of 10^{-3}. Assuming standard surface conditions and four equivalent faces (Fig. 9), I_c (in agreement with experiment) and δI_c^* should be comparable in rods and slabs, except for substituting $4W$ for $2W$ in Eqs. (12) and (46). On writing, like in Eqs. (46) and (47), $\delta\phi_1^*=\delta\phi_2^*=K_1(\mu_0L/2\pi)\delta I_c^*$, we find $K_1\simeq0.7$,[17] so that $\delta\phi_1\sim\delta\phi_z$ in slabs, as observed. Whereas comparable critical-current fluctuations, as sources of noise, give rise to comparable field noises around slabs and rods, the voltage noise is considerably reduced in rods: $S_{VV}\sim10^{-19}$ V^2/Hz. This is explained by smaller flux-flow resistances of rods: the factor R_f^2 appearing in $S_{VV}=R_f^2\delta I_c^{*2}$ is reduced by a factor $(W/t)^2\sim100$. This R_f effect well illustrates the secondary character of the voltage noise as a by product of the surface current fluctuations. It is even more spectacular in a niobium rod. We used a monocrystalline sample of pure niobium: $\rho_n=0.1\ \mu\Omega$ cm $\ll\rho_n$(Pb-In)$=10\ \mu\Omega$ cm. The Nb rod again exhibited similar critical currents and field noise, but no detectable voltage noise. As a matter of fact, for 100 times smaller ρ_f, we expect $S_{VV}\sim10^{-23}$ V^2/Hz. It is worth noting that, in old neutron-diffraction experiments using alike Nb crystals, Thorel and one of us[26] observed the permanence of a quasiperfect vortex crystal in the flux-flow regime. Heiden wrongly ascribed the smallness of δV in Nb to this circumstance. In fact, a strong flux-flow noise is generated near the surface, because of local fluctuations of the vortex curvature over a small layer, which otherwise leave the bulk lattice almost unperturbed.

In this paper we are concerned with the y component of the fluctuating surface current $\mathbf{u}$. In forthcoming experiments, there will be no difficulty in designing pickup coils to investigate the x component of $\mathbf{u}$, and, in particular, to answer the question whether the turbulence is isotropic or not.

C. The magnitude of the flux-flow noise and the length scale of the turbulence

All FFN rms amplitudes [Eqs. (46) and (47)] depend on the intensity of the surface-current turbulence, regarded as the noise sources, through the common factor $(2W/L)^{1/2}u^*c$. This has been interpreted above as the rms fluctuation of the critical current δI_c^*, and is most conveniently measured on integrating the voltage noise spectrum (and dividing by R_f^2). As stated in Sec. VI A, $\delta V^*(0)$, the extrapolated value at low line velocities, can be taken as the representative intensity of the flux-flow voltage noise.

The sample-size dependence of δI_c^*, as $(W/L)^{1/2}$ (for uniform and constant surface conditions) is easily verified. The L dependence of δI_c^* and R_f, giving $\delta V^*\propto L^{1/2}$, corresponds to the rather trivial result that FFN in different segments of the slab are statistically independent, as expected from any model. The W dependence was checked by cutting a slab lengthwise, which is the simplest way of maintaining surface conditions (Fig. 10). While W and I_c were halved ($i_c=I_c/2W=$const), δI_c^* was reduced by a factor of $\sqrt{2}$. Otherwise stated, a value of u^*c is determined, which is independent of the slab dimensions, as it should be, and characterizes a given surface state at given temperature and field.

Strictly, experimental data only give access to the product u^*c. Nevertheless, plotting u^*c and i_c vs B (or vs temperature[17]), suggests that u^* follows any variations of the critical current with field (Fig. 10). This fits in with

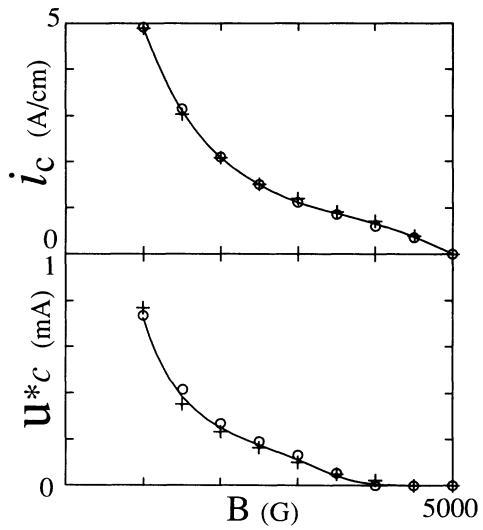

FIG. 10. The upper curve shows the B dependence of the surface critical-current density, defined in Eq. (12) as $i_c\simeq I_c/2W$. For comparison the lower curve shows the B dependence of u^*c, such as deduced through Eq. (46) from the measured intensity of the flux-flow noise voltage. Full lines are fitting lines. Open circles and crosses correspond to data taken at 1.9 K with two PbIn slabs of respective dimensions: (○) $L=30$ mm, $W=10$ mm, $t=0.27$ mm; (+) $L=30$ mm, $W=5$ mm, $t=0.27$ mm. The latter has been cut from the former, so as to preserve given surface conditions.

the idea that $u^* \sim i_c$ in a fully developed turbulence. Thus, letting $u^* = i_c$, we may reasonably estimate a length scale c of the turbulence (Fig. 11). In this way we obtain $c \sim 1$ μm, which is consistent with our starting assumptions ($a \ll c \ll W$). This is an essential point in support of our 2D turbulence model. Just as bundle sizes smaller than φ_0 invalidate the shot noise model, it is clear that unacceptable values of c, say $c \sim 1$ Å or $c \sim 1$ m, would ultimately have invalidated the whole theory, in spite of the foregoing positive results. As a further proof, we have observed that a surface roughness on the scale of 1 μm, such as obtained by spark cutting, entailed marked distortions of the usual smoothly decreasing shape of the FFN spectrum $\Sigma(f)$.

D. Two past experiments reviewed

Jarvis and Park,[8] and independently Choe and Van der Ziel,[7] have measured the induced noise voltage $\dot{\phi}_m$ in a single loop just above the sample surface. They used thin foils (20–50 μm), and pressed a wire of the pickup loop against the foil; the distance of closest approach was about 10–20 μm. In Jarvis and Park's experiments this pickup wire could be raised to a variable height $z' \lesssim 3$ mm above the sample surface. In order to compare some of their results with our own predictions, we shall refer to the arrangement shown in Fig. 12, which allows us to use the notations and results of Sec. IV B: the rectangular loop lies in a plane $x = x'$ ($|x'| < W$), and extends beyond the active "soft" section L of a foil of negligible thickness lying in the plane $z = 0$. Its longitudinal wires (1) and (2) are located at (x',z') where $0 \le z' \lesssim W$, and (x',z'') where $z'' = \infty$ (meaning in practice $z'' \gg W$). Thus, Eq. (28) and subsequent calculations apply. A coupling coefficient $k(x)$ is defined in the same way by Eq. (31), and $K = k(x) - \langle k \rangle_x$. $S_{\phi\phi}$ is then expressed by Eq. (37), where the coefficient $K^{\dagger 2}$, like that of coil C_z, is the x-average value of K^2. $K^\dagger$ has been calculated numerically as function of the loop parameters x' and z' (Figs. 12 and 13).

Jarvis and Park,[8] using a specimen of In-Pb 2 at. %, measured the power spectrum $w(f)$ of $\dot{\phi}_m$, i.e., $f^2 S_{\phi\phi}$, in the range 1–30 kHz. $w(f)$ had a maximum at $f_m \simeq 5$ kHz, and the magnitude of the maximum $w(f_m)$ decreased rapidly with increasing z'. The authors noted

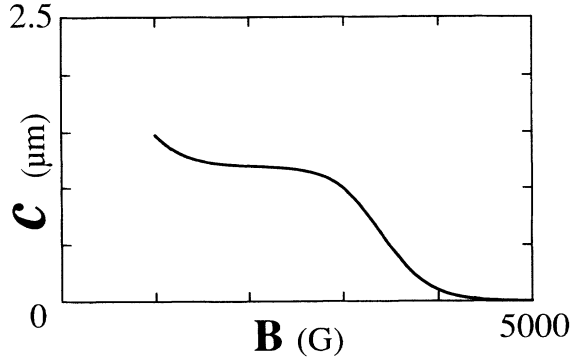

FIG. 11. As explained in the text, assuming $u^* = i_c$, the experimental ratio $u^* c / i_c$ may be taken as an estimation of the length scale c of the turbulence. Here $u^* c / i_c$, standing for c, has been calculated as function of B by using both fitting lines of Fig. 10.

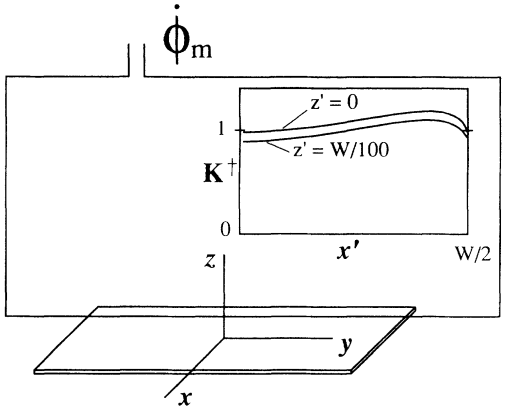

FIG. 12. The sample and coil configuration discussed in Sec. VI C. The sample is a foil of negligible thickness in the horizontal plane $z = 0$. The pickup coil consists in one large rectangular loop in a vertical plane $x' = \text{const}$. The sensing wire of the loop, at (x',z'), lies at a distance z' above the foil surface ($0 \le z' \le W$). The field-noise spectrum $S_{\phi\phi}$ is given by Eq. (37), where $K^{\dagger 2}(x',z')$ is the variance of the associated coupling coefficient. The x' dependence of $K^\dagger$ is shown in the inset for a wire pressed against the surface ($0 \le z' \le W/100$).

that no model of flux motion existed at the time, which could account for this z' dependence. At these frequencies, and in the sample used, $\dot{\phi}_{ms} \sim \dot{\phi}_m$ may be an important term in δV, which now depends on the spatial arrangement of the leads to the voltmeter. Under these conditions, our Eq. (35) for S_{VV} is invalidated, but Eq. (37) for $S_{\phi\phi}$ is not. It should be pointed out, that In-Pb 2 at. % is a type-I material. Moving flux tubes in the intermediate state are presumed to behave like vortices in the mixed state, but the resulting field noise is much stronger.

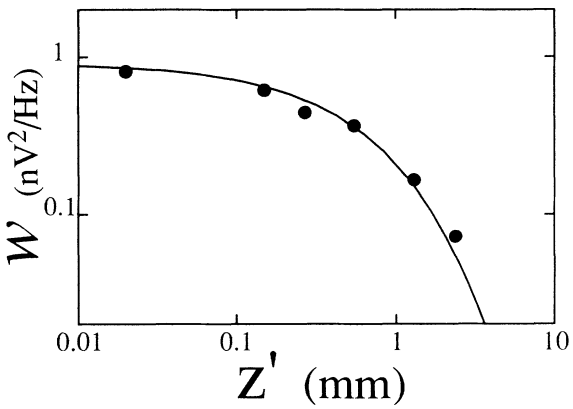

FIG. 13. The power spectrum $w(f) = f^2 S_{\phi\phi}$ of the induced voltage noise through a pickup loop, as measured by Jarvis and Park,[8] using a type-I indium-lead foil, and a potential lead arrangement similar to that shown in Fig. 12. The closest wire parallel to the sample was raised at a variable height z' above the sample surface. Data w vs z' (black points), taken from Fig. 6 of Ref. 8, at $f = 5$ kHz, are plotted in a log-log diagram, like that of Fig. 7 of Ref. 8. According to our model, the z' dependence of w is that of the factor $K^{\dagger 2}$ in $S_{\phi\phi}$, such as given by Eq. (37). The full line is the theoretical curve $K^{\dagger 2}(x' = 0, z')$, except for an arbitrary factor, meaning a simple vertical shift in this diagram.

Jarvis and Park ascribed this fact to the coarser structure of the intermediate state. Anyway, the same model of a 2D turbulence of the currents J (in the plane $z=0$) may be advanced in both cases. As a matter of fact, the z' dependence of $w(f_m)$, as shown in Fig. 13, is well explained by the z' dependence of $K^{\dagger 2}(0,z')$, in accordance with Eq. (37).

Choe and Van der Ziel[7] measured and compared $w(f)$, the power spectrum of $\dot{\phi}_m$, and $S_{VV}(f)$, in pure vanadium foils. Let us consider noise spectra (at 4.2 K, and $B=330$ G) of the sample labeled $P1$ in Ref. 7: its dimensions are $L=16,6$ mm, $W=0,8$ mm, $t=25$ μm, and the flux-flow resistance, as estimated from I-V data of Fig. 8 therein, is $R_f \simeq 1.7$ mΩ. The ratio $\Gamma=w(f)/S_{VV}(f)$ was plotted versus frequency (Fig. 12 of Ref. 7). This plot shows a relationship of the form $\Gamma=\gamma f^2$, and the best fit on logarithmic scales gives $\gamma=2.74\times10^{-10}$; but, from the dispersion of the data, we roughly estimate the bracket $\gamma=(2.7\pm1.2)\times10^{-10}$. So far as we know, Choe and Van der Ziel were the authors who pointed out the unexpected smallness of the field noise when relying on a shot-noise model. Then they considered the unlikely explanation, that the flux-bundle effect could "only hold for the primary noise signal" (i.e., δV), "but not for the secondary noise signal" (i.e., $\delta\dot{\phi}_m$). The simplest argument, supported by experiments, is that flux bundles, as independent entities, do not exist at all. The above relationship clearly means that

$$(S_{\phi\phi}/S_{VV})^{1/2}=\gamma^{1/2}/2\pi=\text{const}=(2.5\pm0.6)\times10^{-6}\ \text{sec}\ ,$$

in the whole frequency range (300 Hz–10 kHz), in agreement with our own results. On substituting Choe and Van der Ziel's data into the second Eq. (37), and taking $K^{\dagger}\simeq1$ ($z'\sim10$ μm, $|x'|<W/2$; see the inset of Fig. 12), we find

$$(S_{\phi\phi}/S_{VV})^{1/2}=(\mu_0 L/2\pi R_f)K^{\dagger}\simeq2\times10^{-6}\ \text{sec}\ .$$

Taking actual experimental conditions into account (all data are not taken in the flux-flow regime; the leads arrangement does not satisfy the condition required in Sec. IV B that $L'\gg L$, or at least $L'\sim2L$), this quantitative agreement is as satisfactory as we could hope.

VII. CONCLUDING REMARKS

Up to then, various interpretations of the FFN were more or less imbued with the shot-noise analogy. Only the supposedly atypical case of pure niobium prompted Heiden *et al.* to attempt another way. On the other hand, the idea of analyzing macroscopic voltages as the sum of contributions of individual vortices, though it is sound, limited one in practice to 2D vortex motions. Combined experimental and theoretical arguments have led us to a quite different approach. Our experiments provide convincing evidence that FFN is not due to randomly nucleated bundles, but to a turbulent flow of surface currents. Accordingly, the shape of the FFN spectrum, $\Sigma(f)$, is not related to any macroscopic transit time such as W/v_L, but to the intricate local dynamics of the vortex array along a rough surface. The bundle concept should be renounced unless we refer now to a group of vortices bending near the surface coherently over a length c. Anyway, this notion makes no sense in the bulk of a soft material. The bulk motion of the vortex array, including the v_L noise, is smoothed and regular, and the more so as samples have large cross sections and low flux-flow resitivities.

The agreement of our results with the detailed predictions of Sec. IV support the correctness of the MS model of the critical state, and the underlying MS continuum theory. The separation of the transport current density into two components $\mathbf{J}_1$ and $\mathbf{J}_2$, which have very different properties (Sec. III A), was an essential point. It allowed us to define the instantaneous critical current I_1 (Sec. III C) and refer to its fluctuations. Otherwise, we could not have imagined the two-step mechanism involved in the voltage noise as described in Sec. III B. The fact that δV can be essentially expressed in terms of bulk δv_L (at $\delta n_L \simeq 0$), implies that the vortex array behaves in the bulk as an incompressible fluid, and responds as a whole to fluctuations of the bulk dissipative current $I_2=I-I_1$. Such spatially coherent δv_L could hardly be conceived as resulting directly from any random distribution of defects. This may explain that earlier theories were inclined to retain fluctuations of the vortex density.

Noise in Joule dissipation is expected to occur as another outcome of the FFN, irrespective of the model involved. As a result, second sound noise is generated in superfluid helium.[25] Detailed second-sound analysis can give information on the spatial distribution and coherence of heat sources. Recently, preliminary results have been obtained by using this technique, which entirely confirm the conclusions of this work.[27] Experimental details are planned to be published elsewhere.

Apart from the fact that a better understanding of the FFN should reestablish it as a useful tool for investigating the dynamics of pinning, the 2D turbulence of surface currents is in itself a new and interesting physical situation. Of course, all questions relevant to the physical origin of the FFN spectrum and correlation length remain open.

ACKNOWLEDGMENT

The "Laboratoire de Physique de la Matière Condensée de l'Ecole Normale Supérieure" is "Unité Associée au CNRS (URA 1437)."

APPENDIX A: 2D VORTEX MOTIONS

Here we consider 2D motions of the vortex array, under conditions defined in Sec. II (straight vortex lines and superposition principle):

$$\boldsymbol{\nu}(0,0,1)\ ;\ n_L(x,y)\ ;\ \mathbf{v}_L\{v_{Lx}(x,y),v_{Ly}(x,y),0\}\ .$$

Let $f(x,y)$ $(-\varphi_0\le f\le\varphi_0)$ be the flux through the measuring circuit of Fig. 1, due to one straight vortex at point (x,y). In view of the context, one should not confuse the flux function f with the frequency. By superposition

$$\phi_{ms}=\int\int f n_L\,dx\,dy\ . \tag{A1}$$

In any geometry, f vanishes along sample edges, for vortices entering or leaving the sample. It has a discontinui-

ty along the line (*asb*) (Fig. 14), with a jump $f_+ - f_- = \varphi_0$ for vortices crossing in the positive x direction.

Using the 2D continuity equation

$$\frac{\partial n_L}{\partial t} + \mathrm{div}\mathbf{J}_L = 0 \quad (\mathbf{J}_L = n_L \mathbf{v}_L) , \tag{A2}$$

the induced voltage term in Eq. (1) reads

$$-\dot{\phi}_{ms} = -\int\int f \frac{\partial n_L}{\partial t} dx\, dy = \int\int f\, \mathrm{div}\mathbf{J}_L dx\, dy . \tag{A3}$$

f is a regular function over a multiply connected region D, the contour of which is shown in Fig. 14. Let $\mathbf{g} = -\nabla f$. As easily seen, $\mathbf{g}$ has no discontinuity along the cut line (*asb*) ($\mathbf{g}_+ = \mathbf{g}_-$), so that $\mathbf{g}$ may be regarded as a well-defined continuous function over the sample surface (excluding singular points a and b). This vector $\mathbf{g}$ can be identified with the Clem's resolving function, as proved by the following derivation, or more directly, though less obviously, from both definitions.

On application of the Stoke's theorem, Eq. (A3) can be rewritten as

$$-\dot{\phi}_{ms} = \int_{asb} (f_- - f_+)(\mathbf{dl} \times \boldsymbol{\nu}) \cdot \mathbf{J}_L + \int\int \mathbf{g} \cdot \mathbf{J}_L dx\, dy . \tag{A4}$$

By substituting $\dot{\phi}_{ms}$ from Eq. (A4) into Eq. (1), we obtain

$$V = \int_{asb} \mathbf{E} \cdot \mathbf{dl} + \int_{asb} \varphi_0 (\mathbf{J}_L \times \boldsymbol{\nu}) \cdot \mathbf{dl} + \int\int \mathbf{g} \cdot \mathbf{J}_L dx\, dy , \tag{A5}$$

since $f_+ - f_- = \varphi_0$. Noting that $\mathbf{E} = -\mathbf{v}_L \times \boldsymbol{\omega} = -n_L \varphi_0 \mathbf{v}_L \times \boldsymbol{\nu}$, the first two terms in Eq. (A5) cancel, leading to the Clem's formula (4).

The magnetic flux ϕ through any pickup coil can be written in the form (A1). Thus the induced voltage can be expressed in the same general form (4) with $\mathbf{g} = -\nabla f$.

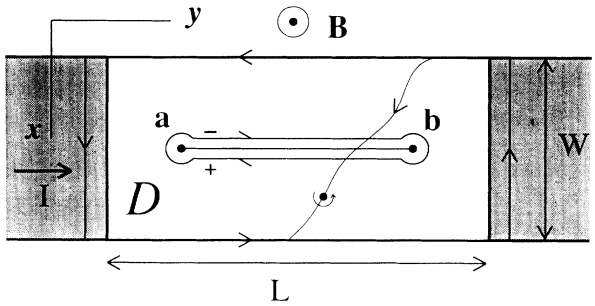

FIG. 14. Assuming 2D vortex motions, the measured voltage using the lead arrangement of Fig. 1 can be calculated from the vortex-current field $\mathbf{J}_L(x,y)$ and a flux function $f(x,y)$, that is the flux through the measuring loop (*ambsa*) due to one vortex located at (x,y). A doubly connected domain D, that is useful in calculations of Appendix A, is defined by the cut line (*asb*) and the rectangular contour $W \times L'$ ($L' > L$) encircling the soft portion of the sample. Along this outer contour, either $\mathbf{J}_L = 0$ or $f = 0$, so that $f\mathbf{J}_L = 0$.

APPENDIX B: CORRELATIONS IN THE TURBULENT-FLOW MODEL

Let us consider two noise signals, A and B, of the general form given in Eq. (34), with respective weighting functions α and β:

$$B = \int\int_{\pm} \beta(x,z) u_y dx\, dy . \tag{B1}$$

The intercorrelation function of A and B can be expressed as

$$C_{AB}(\tau) = \overline{A(t)B(t-\tau)} = \int\int\int\int_{\pm} \alpha(x,z)\beta(x',z) \times \Gamma_{yy}(\mathbf{r}' - \mathbf{r}, \tau) dx\, dy\, dx' dy' . \tag{B2}$$

As remarked in the text (Sec. IV B), cross terms $\overline{u_y^+ u_y^-}$ cancel. Since α and β are slowly varying functions on the scale of the correlation length c, Eq. (B2) can be rewritten as the product

$$C_{AB}(\tau) = \int\int_{\pm} \alpha(x,z)\beta(x,z) dx\, dy \times \int\int_{\pm} \Gamma_{yy}(\mathbf{R}, \tau) dX\, dY . \tag{B3}$$

Here the homogeneous distribution of surface defects is taken into account through the standard form (24) of the current correlation tensor. Using (24) and (25)

$$C_{AB}(\tau) = \sigma_{AB} L W u^{*2} c^2 \chi(\tau) , \tag{B4}$$

where

$$\sigma_{AB} = \langle \alpha\beta \rangle_x^+ + \langle \alpha\beta \rangle_x^- . \tag{B5}$$

The cross spectrum of A and B is

$$S_{AB}(f) = \sigma_{AB} L W u^{*2} c^2 \Sigma(f) . \tag{B6}$$

When dealing with two more or less interrelated random processes, it is often desirable to use a normalized cross-spectral density function $\gamma^2(f)$, known as the *coherence function,* and commonly displayed by signal analyzers. As for A and B,

$$\gamma_{AB}^2 = \frac{|S_{AB}|^2}{S_{AA} S_{BB}} = \frac{\sigma_{AB}^2}{\sigma_{AA} \sigma_{BB}} \leq 1 , \tag{B7}$$

is independent of frequency.

APPENDIX C: NOISE SPECTRA IN A SHOT-NOISE MODEL

Here we assume the same experimental arrangement as specified in Secs. III and IV: voltage probes (a) and (b) attached to the equipotential ends of a long strip, and long rectangular loops including the voltage measuring circuit (*amb*). Under these conditions, the individual vortex flux f, defined in Appendix A, is independent of y, as also the Clem's resolving function g_x in Eq. (5). We thus have

$$\delta V = v_L \int\int g_x(x) \delta n_L dx\, dy , \qquad \delta\phi = \int\int f(x) \delta n_L dx\, dy . \tag{C1}$$

According to a shot-noise model, flux entities or bundles $\varphi_b = q\varphi_0$, are nucleated randomly and move rigidly across the sample at constant speed v_L. The resulting vortex-density correlation function is[14]

$$\overline{\delta n_L(\mathbf{r},t)\delta n_L(\mathbf{r}',t-\tau)} = n_b q^2 \delta(x-x'-v_L\tau)\delta(y-y') , \tag{C2}$$

where n_b is the density of bundles. Eqs. (C1) and (C2) are conveniently extended to the xy plane, it being understood that $f \equiv 0$ and $g_x \equiv 0$ for $|x| > W/2$.

Using Eq. (C2), the intercorrelation function of δV and $\delta\phi$ reduces to

$$C_{V\phi}(\tau) = n_b q^2 v_L L \int\int_{-\infty}^{+\infty} g_x(x) f(x-v_L\tau)dx , \tag{C3}$$

the Fourier transform of which yields the cross-spectral density

$$S_{V\phi} = n_b q^2 L\, G(f/v_L) F^*(f/v_L) , \tag{C4}$$

where G and F are the Fourier transforms of g_x and f, respectively. In the same way, one obtains $S_{VV} = n_b q^2 L v_L GG^*$ and $S_{\phi\phi} = n_b q^2 L/v_L FF^*$. As a straightforward consequence of the above expressions for spectra in terms of products GF^*, FF^*, and GG^*:

$$\gamma^2_{V\phi}(f) = \frac{|S_{V\phi}|^2}{S_{VV}S_{\phi\phi}} \equiv 1 , \tag{C5}$$

meaning that δV *and* $\delta\phi$ *must be fully coherent* for any geometry of the search coil.

Like F and G, S_{VV} and $S_{\phi\phi}$ should not have the same frequency dependence and, furthermore, this depends on the geometry of the measuring loops. The relative amplitude of field and voltage spectra, measured at zero frequency, is

$$\frac{S_{\phi\phi}(0)}{S_{VV}(0)} = \left[\frac{F(0)}{v_L G(0)}\right]^2 = \left[\frac{F(0)}{v_L\varphi_0}\right]^2 , \tag{C6}$$

where $F(0)$ and $G(0)$ are equal to the integrals of $f(x)$ and $g_x(x)$, respectively. From the definition of $\mathbf{g}$, see Appendix A, it is easily seen that, in any case, $G(0) = \varphi_0$.[14] For a rectangular loop $L \times W$ just encircling the sample ($\phi = \phi_s$), one would have $f \equiv \varphi_0$ ($|x| < W/2$) so that $F(0) = \varphi_0 W$ and

$$\left[\frac{S_{\phi\phi}(0)}{S_{VV}(0)}\right]^{1/2} = \frac{W}{v_L} \quad (\phi = \phi_s) . \tag{C7}$$

[1] D. J. Van Oijen and G. J. Van Gurp, Phys. Lett. **17**, 230 (1965).
[2] G. J. Van Gurp, Phys. Rev. **166**, 436 (1968).
[3] C. Heiden, D. Kohake, W. Krings, and L. Ratke, J. Low Temp. Phys. **27**, 1 (1977).
[4] C. Heiden, in *Proceedings of the Thirteenth International Conference on Low Temperature Physics,* edited by K. D. Timmerhaus, W. J. O'Sullivan, and E. F. Hammel (Plenum, New York, 1974), Vol. 3, p. 75; in *Proceedings of the International Discussion Meeting on Flux Pinning in Superconductors,* edited by P. Haasen and H. C. Freyhart (Akademie der Wissenshaften, Göttingen, 1975), p. 300.
[5] D. Kohake and C. Heiden, J. Low Temp. Phys. **40**, 531 (1980).
[6] S. W. Shen and A. Van der Ziel, Physica **64**, 587 (1973).
[7] H. M. Choe and A. Van der Ziel, Physica **84B**, 189 (1976).
[8] P. Jarvis and J. G. Park, J. Phys. F **4**, 1238 (1974).
[9] W. J. Yeh and Y. H. Kao, Phys. Rev. Lett. **53**, 1590 (1984); Phys. Rev. B **44**, 360 (1991).
[10] F. Habbal and W. C. H. Joiner, Phys. Lett. **60A**, 434 (1977); J. Low Temp. Phys. **28**, 83 (1977).
[11] J. D. Thompson and W. C. H. Joiner, Phys. Rev. B **20**, 91 (1979); J. Low Temp. Phys. **37**, 13 (1979).
[12] J. G. Park, J. Phys. C **2**, 742 (1969); J. Phys. F **2**, 957 (1972).
[13] J. R. Clem, Phys. Rev. B **1**, 2140 (1970).
[14] J. R. Clem, Phys. Rep. **75**, 1 (1981).
[15] A. M. Campbell and J. E. Evetts, Adv. Phys. **21**, 199 (1972); **21**, 305 (1972).
[16] P. W. Anderson, Phys. Rev. Lett. **9**, 309 (1962).
[17] B. Plaçais, Ph.D. thesis, Université P. et M. Curie, Paris, 1990.
[18] P. Mathieu and Y. Simon, Europhys. Lett. **5**, 67 (1988).
[19] T. Hocquet, P. Mathieu, and Y. Simon, Phys. Rev. B **46**, 1061 (1992).
[20] B. Plaçais, P. Mathieu, and Y. Simon, Phys. Rev. Lett. **70**, 1521 (1993).
[21] B. Plaçais, P. Mathieu, and Y. Simon, Solid State Commun. **71**, 177 (1989).
[22] Y. B. Kim, C. F. Hempstead, and A. R. Strnad, Phys. Rev. Lett. **13**, 794 (1964).
[23] R. G. Jones, E. H. Rhoderick, and A. C. Rose-Innes, Phys. Lett. **24**, 318 (1967).
[24] D. E. Farrel, B. S. Chandrasekhar, and H. V. Culpert, Phys. Rev. **177**, 694 (1969).
[25] B. Plaçais and Y. Simon, Phys. Rev. B **39**, 2151 (1989).
[26] Y. Simon and P. Thorel, Phys. Lett. **35A**, 450 (1971).
[27] R. Martin, Ph.D. thesis, Université Paris 7, 1992.